

## A Point-by-Point Response to Review Comments

Dr. Yan Yin  
Editor, *Atmospheric Chemistry and Physics*

Dear Dr. Yin,

We are submitting a revised manuscript (#acp-2018-476) for your consideration of publication in *Atmospheric Chemistry and Physics*. We have carefully studied the reviewers' comments and carried out revisions accordingly. Below is a point-by-point response (marked as red) to the review comments. We have also provided a copy of track-change manuscript as well as a clean copy of the revised manuscript.

Thank you for your consideration of this submission. We hope you find our responses adequately address the review comments and the revisions acceptable. We would greatly appreciate it if you could get back to us with your decision at your earliest convenience.

Sincerely,

Cenlin He  
National Center for Atmospheric Research  
Boulder, CO 80301, USA

## **Referee #1**

“The manuscript investigates the effects of snow grain shape and BC-snow mixing states on the snow albedo and surface radiative forcing over the Tibetan Plateau. To achieve the goal, the authors improve the SNICAR model parameterization by introducing nonspherical snow grain shape and BC-snow mixing states based on their previous work, and the parameterization is systematically compared with observations of both pure and polluted snow. Furthermore, the BC observation in the TP is well reviewed, and the uncertainties related to the snow shape and BC-snow mixing are studied. The topic is interesting and important for snow albedo studies, and the manuscript is well organized and written. It can be published on ACP after minor revision.”

We thank the reviewer for his/her constructive comments and suggestions, which help to improve the manuscript. Below is a point-by-point response to the comments.

### **Specific Comments:**

1. Title: The title of the manuscript is not very clear, and the main focus of the paper cannot be clearly obtained through the title. The snow grain shape effects are not related to the BC.

Response: Thank you for the comments. First, we would like to clarify that the snow grain shape effects are closely related to BC impacts on snow albedo. As we showed in this work (and our previous study, He et al. 2018a JGR), spherical snow grains lead to stronger BC-induced albedo reductions than nonspherical snow grains if other conditions/variables are the same. Both snow shape and aerosol-snow mixing state are important to BC-snow albedo effects. In fact, one of our highlights in this work is that the combination of snow grain shape and BC-snow mixing state shows an important interactive effect on BC-induced albedo reduction. Second, the focus of this paper is to assess the uncertainty in BC-induced snow albedo reduction over the Tibetan Plateau caused by snow grain shape and BC-snow mixing state using an improved SNICAR model, which is consistent with the current title. Thus, we think the current title can reflect the focus of the paper and we choose not to change it. Please note that we also put some efforts in describing and evaluating the implementation of new aerosol-snow parameterizations into SNICAR in this paper, because this is the modeling basis for quantifying snow albedo uncertainties over the Tibetan Plateau, which does not deviate from the paper focus.

2. Line 278-287: There are significant uncertainties on BC MAC. The difference between He et al. (2017b) and Bond and Bergstrom (2006) can be simply explained by natural variations. However, the authors made unrealistic adjustment on BC density and size. Is

this really necessary, and how would a different MAC in the model influence the final results?

Response: Thank you for the comments.

First, we agree that the differences in BC MAC between He et al. (2017b) and Bond and Bergstrom (2006) could be due to natural variations/uncertainties. In fact, BC MAC could vary from  $\sim 2$  to  $\sim 15 \text{ m}^2 \text{ g}^{-1}$  due to uncertainties in particle density, size, structure, and refractive index. However, based on a comprehensive review of observations, Bond and Bergstrom (2006) recommended a value of  $7.5 \text{ m}^2 \text{ g}^{-1}$  at 550 nm to best represent BC MAC, which has been widely adopted in previous studies (e.g., Aoki et al., 2011; Flanner et al., 2007, 2009). Thus, to reduce the potential uncertainty from BC MAC in this work, we have chosen to use the value recommended by Bond and Bergstrom (2006).

Second, to achieve the recommended BC MAC, we adjusted the BC density to be  $1.5 \text{ g cm}^{-3}$  and BC size to be a lognormal distribution with a geometric mean diameter of  $0.06 \mu\text{m}$  and a geometric standard deviation of 1.5. We would like to clarify that these values are reasonable for BC particles. (1) In fact, a BC density of  $1.5 \text{ g cm}^{-3}$  has been widely used in previous studies (e.g., Flanner et al. 2007; Aoki et al., 2011), as indicated in the manuscript. Bond and Bergstrom (2006) suggested that the measured void-free BC usually has a density of  $1.7\text{--}1.9 \text{ g cm}^{-3}$  but the density can be lower for BC with voids. Long et al. (2013) further showed that ambient BC particle density can vary from  $1.2$  to  $1.8 \text{ g cm}^{-3}$ . (2) The BC size used in this work is also within the observed ranges. Bond et al. (2006) showed that the observed BC geometric mean diameter varies from  $0.01$  to  $0.15 \mu\text{m}$  near combustion sources, while the observed geometric standard deviation varies from 1.2 to 2.0 for BC either near combustion sources or in continental plumes.

Third, if using a smaller BC MAC (e.g.,  $6.8 \text{ m}^2 \text{ g}^{-1}$  at 550 nm as used in He et al. 2017b), the BC-induced snow albedo reduction would be smaller, compared with current estimates using a value of  $7.5 \text{ m}^2 \text{ g}^{-1}$ . The quantification of MAC effects on snow albedo reduction is beyond the scope of this study and will be investigated in future work.

To clarify, we have included the aforementioned discussions in the track-change manuscript (Lines 292–302) as follows:

*“We should note that BC MAC could vary significantly in reality (e.g., from 2 to 15  $\text{m}^2 \text{ g}^{-1}$  at 550 nm) due to uncertainties from particle density, size, structure, and refractive index (Bond and Bergstrom, 2006). Thus, we use the recommended value ( $7.5 \text{ m}^2 \text{ g}^{-1}$ ) derived from a comprehensive review of measurements to reduce the potential uncertainty from BC MAC in this study. Compared with the current estimates, using a smaller BC MAC (e.g.,  $6.8 \text{ m}^2 \text{ g}^{-1}$  at 550 nm as used in He et al. 2017b) would lead to weaker BC-induced snow albedo reductions, the quantification of which, however, is beyond the scope of this study and will be investigated in future work. In addition, the adjusted BC density and size used in the present study are still within the observed ranges, with  $1.2\text{--}1.9 \text{ g cm}^{-3}$  for densities (Bond and Bergstrom, 2006; Long et al., 2013) as well as  $0.01\text{--}0.15$*

*μm and 1.2–2.0 for geometric mean diameters and standard deviations (Bond et al., 2006), respectively.”*

3. Table 1: The authors made some assumptions to evaluate the new parameterization, and Table 1 list most parameters for comparison with observations. The detailed assumptions should be indicated in the manuscript, e.g., which parameters are assumed, and which parameters are observed. Meanwhile, are the parameters adjusted to match the observations, or realistic parameters that are picked independent of observations lead to the great agreement.

Response: Thank you for the comments. We would like to clarify that all the parameter values are picked based on the corresponding observed/realistic values in each case when the observations are available. We did not adjust model parameters to match observations. Even for the assumed parameter values indicated in Table 1, we did not tune the values to match observations. Instead, we adopted either commonly used values or observed values from other studies. Following the reviewer’s comment, we have included the detailed assumptions and clarifications in the track-change manuscript as follows:

Lines 332-346: *“To conduct reasonable comparisons, we used the observed snow density, grain size, thickness, snowpack layer, direct/diffuse radiation, solar zenith angle, and underlying ground albedo in model simulations for each case (see Table 1 and Figure 6 for details), except for underlying ground albedos in the Brandt et al. (2011) and Painter et al. (2007) cases and the grain size of the second snow layer in the Brandt et al. (2011) case because of unavailable measurements. Thus, we assumed black underlying grounds (albedo = 0) in the two cases, which has negligible effects on albedo estimates due to thick snow optical depths. In the Brandt et al. (2011) case, we further assumed an effective radius of 500 μm (typical for aged snow) in the second snow layer to make it optically semi-infinite, which is consistent with the observed condition.”*

Lines 386-395: *“Similar to Section 3.4.1, we used the observed BC concentration in snow, snow density, grain size, thickness, snowpack layer, direct/diffuse radiation, solar zenith angle, and underlying ground albedo in model simulations for each case (see Table 1 and Figure 7 for details), except for the snow density in the Pedersen et al. (2015) case and the underlying ground albedo in the Meinander et al. (2013) case because of unavailable measurements. Thus, we assumed a typical fresh snow density of 150 kg m<sup>-3</sup> in the former case and a black underlying ground (albedo = 0) in the latter case. Compared with assuming a black underlying ground, we find that using a non-black underlying ground albedo typically observed over the Tibet (Qu et al., 2014) only leads to very small (<5%) relative differences in albedo calculations in the Meinander et al. (2013) case.”*

4. Figure 6: It seems that most observations give an albedo slightly less than 1 around 400nm, whereas most model results overestimate the albedo. Is there any explanation?

Response: Thanks for pointing it out. The slight but systematic model overestimates at around 400 nm (shown in Fig. 6) are probably due to the uncertainty of ice refractive indices. Based on a recent study (Picard et al., 2016), the ice refractive indices (Warren and Brandt, 2008) used in this study may result in too weak snow absorption around 400 nm and hence lead to albedo overestimates, compared with observations. We have included the following discussions in the track-change manuscript (Lines 368–380):

*“We note that model results in all cases show slight but consistent albedo overestimates around 400 nm compared with observations (Fig. 6), probably due to the uncertainty of ice refractive indices. In this work, we used ice refractive indices from the most widely-used database (Warren and Brandt, 2008) obtained from measurements in the Antarctic, which shows a very low ice absorption coefficient around 400 nm. However, based on more recent measurements in Antarctic snow, Picard et al. (2016) found a much higher ice absorption coefficient around 400 nm than that from Warren and Brandt (2008), which suggested that the uncertainty in ice visible absorption is probably larger than generally appreciated. Therefore, the weak snow absorption caused by refractive indices used in this study could lead to the overestimates in modeled albedo around 400 nm.”*

5. Figure 8: The effects on the snow albedo and surface radiative effects are illustrated in the figure. The two variables are closely related, and, from the figure, it seems that there is a strong correlation between them.

Response: Yes, the BC-induced snow albedo reduction is closely correlated with the surface radiative effects. This is because the regional mean surface radiative effect is computed by multiplying the regional mean snow albedo reductions with the regional mean surface downward solar fluxes (from MERRA-2 reanalysis data). As shown in Table S2 (in the supplement), the mean surface downward solar fluxes across different Tibetan sub-regions are similar during the same season, which leads to the strong correlation between snow albedo reductions and surface radiative effects across the sub-regions as shown in Fig. 8.

6. The manuscripts show significant influences of snow shape and BC-snow mixing on surface albedo. During the discussion, the albedo reductions, which are relatively small, are used to evaluate the influence. The surface albedos under different circumstances can directly compared to indicate the influences. Furthermore, considering the variations on the models and input parameters, the uncertainties on the albedo may be quite significant, and this may greatly influence the conclusions.

Response: Thank you for the comments. We agree that the present estimates of albedo reductions may be associated with uncertainties from various factors, including model and input parameters, which could affect the signal of BC-induced albedo reductions. Besides, in relatively clean areas, the BC-induced albedo reductions are small (e.g.,

<0.01), which may be comparable or even smaller than the uncertainty of surface/snow albedo under different conditions. Surface albedos obtained from remote sensing observations typically have errors of a few percent (Warren, 2013 JGR). However, in the polluted regions, the albedo reductions can be larger than 0.1, which provides strong and detectable signals. In this study, to reduce the uncertainty in albedo calculations, we have used observed values for model/input parameters in the estimates of BC-induced albedo reductions over TP when measurements are available. However, we do realize that there are still several important uncertainty sources and limitations in this study, including uncertainties from measurements, BC and snow grain properties, and complex snowpack processes, which have been discussed in the original manuscript (Lines 470–482). Here, we have further included discussions on the uncertainty issues mentioned by the reviewer in the track-change manuscript (Lines 533–536) as follows:

*“These uncertainties associated with modeling and measurements may decrease the signal-to-noise ratio for the detection of BC effects on snow albedo, particularly in relatively clean regions with small BC-induced albedo reductions (e.g., <0.01). Thus, improved and robust estimates require both accurate snow albedo modeling and snowpack measurements.”*

7. The manuscript includes a lot of information and leads to a few quite important conclusions. The conclusion section seems simply a list of the work done and conclusions obtained. A lot of details are included in the section, but it is not well organized. It should definitely be re-organized to better summary the focus of the manuscript.

Response: Thank you for the comments. We have re-organized and refined the conclusion section to better summarize and highlight the focus of this study as follows (Lines 544–617):

*“ We implemented a set of new BC-snow parameterizations into SNICAR, a widely used snow albedo model, to account for the effects of snow nonsphericity and BC-snow internal mixing. We evaluated model simulations by comparing with observations. We further applied the updated SNICAR model with a comprehensive set of in-situ measurements of BC concentrations in the Tibetan Plateau (TP) snowpack (glacier) to quantify the present-day BC-induced snow albedo effects and associated uncertainties from snow grain shape and BC-snow mixing state.*

*Based on the SNICAR model updated with new BC-snow parameterizations, we found that nonspherical snow grains tend to have higher pure albedos but lower BC-induced albedo reductions compared with spherical snow grains, while BC-snow internal mixing substantially enhances albedo reductions relative to external mixing. Compared with observations, model simulations assuming nonspherical snow grains and BC-snow internal mixing perform better than those with the common assumption of snow spheres and external mixing. The results suggest an important interactive effect from snow*

*nonsphericity and internal mixing, and highlight the necessity of concurrently accounting for the two factors in snow albedo and climate modeling.*

*We further applied the updated SNICAR model with comprehensive in-situ observations of BC concentrations in snow and snowpack properties over the TP to quantify the present-day (2000–2015) BC-induced snow albedo effects. We found that BC concentrations show distinct sub-regional and seasonal variations. The concentrations are generally higher in the non-monsoon season and low-altitudes (<5200 m) than in the monsoon season and high-altitudes (>5200 m), respectively. The spatiotemporal distributions of snow albedo reductions and surface radiative effects generally follow that of BC concentrations. As a result, the BC-induced mean albedo effects vary by up to an order of magnitude across different sub-regions and seasons, with values of 0.7–30.7 (1.4–58.4)  $W m^{-2}$  for BC externally mixed with fresh (aged) snow spheres.*

*Moreover, the BC-snow albedo effects over the TP are significantly affected by the uncertainty in snow grain shape and BC-snow mixing state. We found that BC-snow internal mixing enhances the mean albedo effects by 30–60% relative to external mixing across different sub-regions and seasons, while nonspherical snow grains reduce the albedo effects by up to 31% relative to spherical grains. These effects become comparably important with the snow aging/size effect over polluted areas. Therefore, the combined effects of snow grain shape and BC-snow mixing state can complicate the spatiotemporal features of BC-snow albedo effects over the TP, with significant implications for regional hydrological processes and water management.*

*In summary, this study points toward an imperative need for improved measurements and model characterization of snow grain shape and aerosol-snow mixing state in order to accurately estimate BC-induced snow albedo effects. In future work, we will incorporate the new features of the updated SNICAR model into land surface and climate models, including CESM-Community Land Model (CLM) for global modeling and WRF-Noah-MP for regional modeling, to account for the effects of snow grain shape and aerosol-snow mixing state and to assess the associated uncertainties and hydrological feedbacks in global/regional climate system.”*

## **Referee #2**

“In this paper, the authors study the impact of snow grain shape and black carbon (BC)-in-snow mixing state on snow albedo and BC-snow radiative effects. The authors update the SNICAR model by introducing new sets of parameterizations for snow optical properties based on snow grain shape and BC-in-snow mixing state. The updated SNICAR model is used to reproduce spectral observations of pure and BC contaminated snow, and is applied to field observations across Tibetan Plateau to illustrate the impact of snow grain shape and BC-in-snow mixing state on regional BC-snow radiative effects. The discussions and figures are clear and well organized in general.”

We thank the reviewer for his/her constructive comments and suggestions, which help to improve the manuscript. Below is a point-by-point response to the comments.

### **Specific Comments:**

1. Table 1: For field observations that did not measure underlying ground albedo, the authors assume an albedo of 0 for SNICAR computation; while the underlying ground albedo rarely reach 0 even for dark soil. The snow depth for some of these measurements is shallow, that some light may penetrate through the snowpack. Is there any reason that the authors assigned 0? Perhaps consider adjusting underlying ground albedo to see if this will impact the comparisons show in Figure 6 and 7.

Response: Thank you for the comments. We have conducted additional sensitivity simulations for the three cases without measurements of underlying ground albedo by using values of 0.1 and 0.2 for visible and NIR bands, respectively, based on observations over the TP. For the Painter et al. (2007) and Brandt et al. (2011) cases, the differences by using different underlying ground albedos are negligible due to thick snow optical depths. For the Meinander et al. (2013) case with relative thin snow layers, the relative differences by using different underlying ground albedos are still small (<5%) due to large snow grain sizes and hence thick optical depths. We have included these discussions in the track-change manuscript as follows:

Lines 337–338: “Thus, we assumed black underlying ground (albedo = 0) in the two cases, which has negligible effects on albedo estimates due to thick snow optical depths.”

Lines 392–395: “Compared with assuming a black underlying ground, we find that using a non-black underlying ground albedo typically observed over the Tibet (Qu et al., 2014) only leads to very small (<5%) relative differences in albedo calculations in the Meinander et al. (2013) case.”

2. Table 1: For field studies that report snow effective radius, how did they define/measure/derive the snow effective radius? Do they use similar assumptions as the spherical snow grain in SNICAR?

Response: Thank you for the comments. Snow grain sizes reported by the field studies are retrieved by different methods. For the Painter et al. (2007), Hadley and Kirchstetter (2012), and Pedersen et al. (2015) cases, they retrieved snow grain sizes by matching results of snow radiative transfer models with measured NIR snow albedo spectra. For the Grenfell et al. (1994), Meinander et al. (2013), and Svensson et al. (2016) cases, they determined snow grains sizes by visual estimates with tools (e.g., hand lens with macro-photograph or mm-grids with magnifier). We note that these different measuring methods could introduce uncertainties to the measured snow grain sizes. Moreover, the snow grain size from visual estimates in field studies also differs from the snow effective size (i.e., surface area-weighted mean radius) defined in SNICAR, which could introduce additional uncertainties to snow albedo calculations and comparisons with observations. We have included these discussions in the revised manuscript (Lines 428–434) as follows:

*“We note that the snow grain sizes reported by the aforementioned field studies are retrieved by different methods, including matching snow model results with measured albedo spectra (Painter et al., 2007; Hadley and Kirchstetter, 2012; Pedersen et al., 2015) and visual estimates with tools (Grenfell et al., 1994; Meinander et al., 2013; Svensson et al., 2016) that are not equivalent to the snow effective size (i.e., surface area-weighted mean radius) defined in SNICAR. This could introduce uncertainties to snow albedo calculations and model-observation comparisons.”*

3. Lines 325-326: the authors say they “made reasonable assumptions for cases when measurements are absent”. The readers may wonder what are these “reasonable assumptions” and how did authors justify these assumptions. Perhaps including some details on, for example, how to assign underlying ground albedo (comment 1) when measurement is absent, and etc.

Response: Thank you for the comments. Following the reviewer’s suggestion, we have included more details, including which parameters are based on observed values and which parameters are assumed as well as some justifications of these assumptions. We have also conducted sensitivity simulations to investigate effects of assumed underlying ground albedo (see the response to Comment #1). The additional discussions have been included in the track-changed manuscript (Lines 332–346 and 386–395). Please see the response to Reviewer #1, Comment #3 for details.

4. Table 2: The zeros in albedo reduction values can be distracting that prevent direct comparisons across regions; perhaps consider keeping only the non-zero digits and modify the unit.

Response: Thanks for the comment. Following the reviewer's suggestion, we have modified the values using the expression of scientific notation in the revised Table 2.

5. Lines 340-342: in Figure 6a, as the authors mentioned, the snow grains created in Hadley and Kirchstetter (2012) tend to be spherical, yet the nonspherical grain assumption yields better results. What does this imply for future modeling/field works regarding snow grain shape and snow grain size? Does this mean even if the snow grain shape is relatively well observed in the field, the snow radiative transfer modeling based off the observed grain shape may not improve the snow modeling? Or in another word, to what extent should radiative modeling rely on field observed snow grain shapes since it seems, from figure 6b, the model can always adjust snow grain size to match observations, no matter what grain shape it adopted.

Response: Thanks for the comments.

(1) The snow grains created in Hadley and Kirchstetter (2012) tend to be spherical. However, based on their microscopic images (Fig. S3 in their study), the grains are not perfectly spherical and there are still a portion of grains with either spheroid or aggregating shapes. This is probably why assuming nonspherical grains in our model yields slightly better results than assuming purely spherical grains (Fig. 6a in this study).

(2) Our results do not imply that the snow albedo modeling based on observed grain shape may not improve model results. Instead, one of our key findings/points in this study is that it is necessary to account for realistic/observed snow grain shape in order to accurately estimate snow albedo, which has been supported by the improved model results using nonspherical snow grains (see Sect. 3.4). However, each parameter used in snow modeling could be associated with uncertainties. It is likely that using the observed grain shape may not improve model results when the uncertainties/biases in other model parameters are large. Thus, accurate estimates of snow albedo require constraining all the model parameters together by observations. In summary, this study points toward an imperative need for improved measurements and model characterization of snow shapes.

(3) We agree that the snow grain size can always be adjusted to make model results match observations, whatever the grain shape is assumed. However, this could lead to the issue of getting right answers (e.g., albedo) for wrong reasons (e.g., grain size) due to the lack of grain shape information. Moreover, we have shown that assuming different snow grain shapes can lead to substantial variations in the optimal grain sizes determined by matching observed albedo spectra (Figs. 6b and 7d). This highlights the necessity of accounting for realistic grain shapes in snow size retrievals, which can effectively reduce the uncertainty in retrieved grain sizes. In addition, for the purpose of weather and climate forecasts, snow and climate modeling rely on observed/realistic snow grain shape to produce accurate albedo predictions and associated climate feedbacks.

6. Figure 6b and 7d: it seems that the model simulations fail to capture the drop of snow albedo around 0.25 um observed by Brandt et al., 2011. Is there any explanation?

Response: Thanks for pointing it out. This is because of the uncertainty in ice refractive indices at short wavelengths. The ice refractive indices used in this study result in too weak snow absorption at wavelengths <400 nm and hence lead to model overestimates in albedo at these wavelengths. We have included the discussions in the track-change manuscript (Lines 368–380). Please see the response to Reviewer #1, Comment #4 for details.

### **Referee #3**

“The authors implement a set of new parameterizations in the widely used SNICAR model to account for effects of snow grain shape and the mixing state of BC-snow. Then, they apply the updated SNICAR model with in-situ measurements of BC concentrations in the Tibetan Plateau snowpack to quantify the present-day snow albedo effects. Generally, the results are of great significance, and it’s a very interesting paper with well written, and the expression is clear. I suggest that this manuscript could be accepted with minor revisions.”

We thank the reviewer for his/her constructive comments and suggestions, which help to improve the manuscript. Below is a point-by-point response to the comments.

#### **Minor Comments:**

1. My major concern is that the historical snow sampling sites are very limited in the TP regions, and some of the sampling sites are only representative the high glacier regions. The author should be very careful to use the surface measurement to represent the regional averages. So I don’t think it is quite useful to divide the entire TP and surrounding areas into six subregions as shown in Figure 1 and Table 2.

Response: Thanks for the comments. We agree that the snow sampling sites are very limited over the TP and may not be representative for the entire TP region. This is why we have divided the entire TP domain into six smaller sub-regions for analysis. Within each sub-region, we found that BC concentrations show distinct altitudinal and seasonal variations. Thus, we have further divided each sub-region into high-/low-altitude areas and monsoon/non-monsoon seasons for analysis. As such, we tried to reduce the uncertainty from sample representativeness. Therefore, we believe that dividing the entire TP into smaller sub-regions is still useful. However, we do realize that even after dividing the sub-regions, the current observations in each sub-region are still limited, which may introduce uncertainty in the analysis and highlights an urgent need for more extensive measurements in the region. We have included these discussions in the manuscript (Lines 181–185) as follows:

*“We note that the current observations over the TP are still rather limited spatially and temporally, leading to questions of representativeness and introducing uncertainty in the analysis. Thus, the large sub-regional, altitudinal, and seasonal heterogeneity of BC concentrations in the TP snowpack highlights an urgent need for extensive measurements.”*

2. The conclusion is a little repetitive, which should be reconstructed.

Response: Thanks for the comments. We have re-organized and refined the conclusion section to better summarize and highlight the focus of this study (Lines 544–617). Please see the response to Reviewer #1, Comment #7 for details.

1 **Black carbon-induced snow albedo reduction over the Tibetan Plateau: Uncertainties from**  
2 **snow grain shape and aerosol-snow mixing state based on an updated SNICAR model**

3

4 Cenlin He<sup>1,2</sup>, Mark G. Flanner<sup>3</sup>, Fei Chen<sup>2,4</sup>, Michael Barlage<sup>2</sup>, Kuo-Nan Liou<sup>5</sup>, Shichang Kang<sup>6,7</sup>,  
5 Jing Ming<sup>8</sup>, and Yun Qian<sup>9</sup>

6

7 <sup>1</sup>Advanced Study Program, National Center for Atmospheric Research, Boulder, CO, USA

8 <sup>2</sup>Research Applications Laboratory, National Center for Atmospheric Research, Boulder, CO, USA

9 <sup>3</sup>Department of Climate and Space Sciences and Engineering, University of Michigan, Ann Arbor, MI,  
10 USA

11 <sup>4</sup>State Key Laboratory of Severe Weather, Chinese Academy of Meteorological Sciences, Beijing, China

12 <sup>5</sup>[Joint Institute for Regional Earth System Science and Engineering](#), and Department of Atmospheric and  
13 Oceanic Sciences, University of California, Los Angeles, CA, USA

14 <sup>6</sup>State key laboratory of Cryospheric Science, Northwest Institute of Eco-Environment and Resources,  
15 Chinese Academy of Sciences, Lanzhou, China

16 <sup>7</sup>CAS Center for Excellence in Tibetan Plateau Earth Sciences, Beijing, China

17 <sup>8</sup>Multiphase Chemistry Department, Max Planck Institute for Chemistry, Mainz, Germany

18 <sup>9</sup>Atmospheric Sciences and Global Change Division, Pacific Northwest National Laboratory, Richland,  
19 WA, USA

20

21 \*The National Center for Atmospheric Research is sponsored by the National Science Foundation.

22

23

24

25 *Correspondence to:* Cenlin He (cenlinhe@ucar.edu)

26

27

28

29

30

31

32

Formatted: Font: 11 pt

Deleted: ¶

34 **Abstract**

35 We implement a set of new parameterizations into the widely used SNow, ICe, and Aerosol  
36 Radiative (SNICAR) model to account for effects of snow grain shape (spherical versus  
37 nonspherical) and black carbon (BC)-snow mixing state (external versus internal). We find that  
38 nonspherical snow grains lead to higher pure albedo but weaker BC-induced albedo reductions  
39 relative to spherical snow grains, while BC-snow internal mixing significantly enhances albedo  
40 reductions relative to external mixing. The combination of snow nonsphericity and internal mixing  
41 suggests an important interactive effect on BC-induced albedo reduction. Comparisons with  
42 observations of clean and BC-contaminated snow albedo show that model simulations accounting  
43 for both snow nonsphericity and BC-snow internal mixing perform better than those using the  
44 common assumption of spherical snow grains and external mixing. We further apply the updated  
45 SNICAR model with comprehensive *in-situ* measurements of BC concentrations in the Tibetan  
46 Plateau snowpack to quantify the present-day (2000–2015) BC-induced snow albedo effects from  
47 a regional and seasonal perspective. The BC concentrations show distinct and substantial sub-  
48 regional and seasonal variations, with higher values in the non-monsoon season and low altitudes.  
49 As a result, the BC-induced regional mean snow albedo reductions and surface radiative effects  
50 vary by up to an order of magnitude across different sub-regions and seasons, with values of 0.7–  
51 30.7 (1.4–58.4) W m<sup>-2</sup> for BC externally mixed with fresh (aged) snow spheres. The BC radiative  
52 effects are further complicated by uncertainty in snow grain shape and BC-snow mixing state. BC-  
53 snow internal mixing enhances the mean albedo effects over the plateau by 30–60% relative to  
54 external mixing, while nonspherical snow grains decrease the mean albedo effects by up to 31%  
55 relative to spherical grains. Based on this study, extensive measurements and improved model  
56 characterization of snow grain shape and aerosol-snow mixing state are urgently needed in order  
57 to precisely evaluate BC-snow albedo effects.

58  
59  
60  
61  
62  
63  
64

65 **1. Introduction**

66 Snow albedo, a critical element in the Earth and climate system, can be significantly  
67 affected by light-absorbing impurities in snow (Warren and Wiscombe, 1980; Hansen and  
68 Nazarenko, 2004; Jacobson, 2004; Flanner et al., 2009; Liou et al., 2014), which further influences  
69 surface energy flux and regional hydrological cycles (Menon et al., 2010; Qian et al., 2011, 2015)  
70 through a positive snow albedo feedback (Qu and Hall, 2006). With the strongest light-absorbing  
71 ability, black carbon (BC) has been identified as one of the most important contributors to snow  
72 albedo reduction and snow melting after its deposition onto global snowpack (Ramanathan and  
73 Carmichael, 2008; Bond et al., 2013), including over the Arctic (McConnell et al., 2007;  
74 Meinander et al., 2013), North American mountains (Qian et al., 2009; Sterle et al., 2013; Skiles  
75 and Painter, 2016; Wu et al., 2018), European glaciers (Painter et al., 2013; Di Mauro et al., 2017),  
76 Asian seasonal snowpack (Wang et al., 2013, 2017; Zhao et al., 2014), and the Tibetan Plateau  
77 (Xu et al., 2009; Qian et al., 2011; Wang et al., 2015; Lee et al., 2017; Li et al., 2017, 2018; Zhang  
78 et al., 2017a, b, 2018). In addition, snow albedo can be affected by snow grain size, grain shape,  
79 and snowpack structures (Wiscombe and Warren, 1980; Flanner et al. 2007; Kokhanovsky, 2013;  
80 Liou et al., 2014; Qian et al., 2014; He et al., 2017a; Räisänen et al., 2017), which complicates the  
81 BC-snow-radiation interactions. Thus, it is critically important to account for the effects of snow  
82 grain properties and BC particles in order to accurately estimate snow albedo and subsequent  
83 hydro-climatic impacts.

84 The Tibetan Plateau (TP), also known as the Third Pole, is covered by the largest mass of  
85 snow and ice outside the Arctic and Antarctic (Kang et al., 2010; Yao et al., 2012). It is the source  
86 region of major Asian rivers, providing fresh water for billions of people (Qin et al., 2006;  
87 Immerzeel et al., 2010). Meanwhile, because of its thermal heating, the TP has profound dynamical  
88 influences on the atmospheric circulation in the Northern Hemisphere and long been identified to  
89 be critical in regulating the Indian and East Asian monsoons (Manabe and Terpstra, 1974; Yeh et  
90 al., 1979; Yao et al., 2012). The TP is very sensitive to the change in snow albedo and cover, which  
91 alter surface heat and water balances and further disturb the Asian hydrological cycle and monsoon  
92 climate (Kang et al., 2010). Observations have shown substantial BC concentrations in snow over  
93 the TP and suggested that BC deposition is an important driver of strong albedo reductions and  
94 accelerated glacier retreat in the region (Ming et al., 2008, 2013; Xu et al., 2009; Qu et al., 2014;  
95 Ji et al., 2015; Niu et al., 2017; Li et al., 2017b; Zhang et al., 2018). Recent studies found that BC

96 particles over the TP are primarily from South and East Asia, while long-range transport from  
97 northern mid-latitudinal source regions outside Asia also has nontrivial contributions (Kopacz et  
98 al. 2011; Lu et al., 2012; He et al., 2014a, b; Zhang et al., 2015; Li et al., 2016; Yang et al., 2018).

99 To estimate BC-induced snow albedo effects over the TP, previous studies often used  
100 observed BC concentrations in snow/ice as inputs to snow albedo models by assuming spherical  
101 snow grains and BC-snow external mixing (e.g., Ming et al., 2013; Jacobi et al., 2015; Schmale et  
102 al., 2017; Zhang et al., 2018). This simplified treatment of BC-snow interactions has been widely  
103 used in snow albedo modeling over various snow-covered regions (e.g., Warren and Wiscombe,  
104 1980; Flanner et al., 2007; Aoki et al., 2011). However, snow grains are usually nonspherical  
105 (Dominé et al., 2003) and internally mixed with BC particles (Flanner et al., 2012) in real  
106 snowpack, which could significantly affect BC-snow albedo effects. For example, Kokhanovsky  
107 and Zege (2004) pointed out that substantial errors could occur if assuming spherical snow grains  
108 in albedo modeling. Dang et al. (2016) found that, compared with spherical snow grains, the  
109 nonspherical counterparts lead to higher pure snow albedo but smaller BC-induced albedo  
110 reduction for BC-snow external mixing. In addition, Flanner et al. (2012) showed that there could  
111 be up to 73% of BC in global snowpack internally mixed with snow grains, which increases BC-  
112 induced albedo effects by up to 86% relative to purely external mixing for spherical snow grains.  
113 Moreover, recent studies (He et al., 2014b, 2018a; Liou et al., 2014), combining both effects of  
114 snow nonsphericity and BC-snow internal mixing, revealed that the enhancement in snow albedo  
115 reduction caused by internal mixing can be weakened by snow nonsphericity effect. Therefore,  
116 ignoring these two critical factors in previous studies could lead to biased estimates of BC-induced  
117 snow albedo effects over the TP and elsewhere, which highlights the necessity of accounting for  
118 the two features together in snow albedo modeling and assessing the associated uncertainty.

119 In this study, we implement a set of new BC-snow parameterizations (He et al., 2017b)  
120 into the widely used SNow, ICe, and Aerosol Radiative (SNICAR) model (Flanner et al., 2007) to  
121 consider the effects of snow nonsphericity and BC-snow internal mixing. We further apply the  
122 updated SNICAR model with a comprehensive set of *in-situ* measurements of BC concentrations  
123 in the TP snowpack to estimate the present-day (2000-2015) BC-induced snow albedo effects and  
124 associated uncertainties from snow grain shape (spherical versus nonspherical) and BC-snow  
125 mixing state (external versus internal) from a regional and seasonal perspective. To the best of our  
126 knowledge, this is the first attempt to quantify BC-snow albedo effects over the TP by taking into

127 account the aforementioned two factors concurrently with observational constraints. We describe  
128 BC observations in the TP snowpack in Section 2. We implement the BC-snow parameterizations  
129 and evaluate model results in Section 3. We further quantify and discuss the BC-snow albedo  
130 effects and associated uncertainties in Section 4. Finally, we present conclusions, implications,  
131 and future work in Section 5.

132

## 133 **2. BC observations in the Tibetan snowpack**

134 We collect available *in-situ* observations of BC concentrations in snow/ice over the TP and  
135 surrounding areas during 2000–2015 from historical measurements (see Table S1 for summary).  
136 Although the features of BC concentrations at each site have been described in detail by previous  
137 observational studies, the present analysis seeks to summarize all these measurements in order to  
138 understand the regional and seasonal characteristics of BC pollution in the TP snowpack and more  
139 importantly to estimate the corresponding BC-snow albedo effects and associated uncertainties  
140 due to snow grain shape and BC-snow mixing state using an updated snow model (see Section 3).

141 For detailed analyses, we divide the entire TP and surrounding areas into six sub-regions  
142 (Fig. 1), including northwestern TP (NWTP; 34–40°N, 70–78°E), north of TP (NOTP; 40–45°N,  
143 70–95°E), northeastern TP (NETP; 34–40°N, 95–105°E), southeastern TP (SETP; 27–34°N, 95–  
144 105°E), central TP (CTP; 30–36°N, 78–95°E), and the Himalayas (HIMA). We note that NOTP  
145 represents the Tianshan region. Due to its proximity to the TP, we analyze it together with the TP  
146 snowpack in this study. Moreover, BC concentrations in the TP snowpack show distinct altitudinal  
147 and seasonal variations within each sub-region (Figs. 1a–1f), with much larger values at relatively  
148 lower altitudes (<5200 m a.s.l.) and in the non-monsoon season (October–May; Xu et al., 2009),  
149 compared with higher altitudes (>5200 m a.s.l.) and the monsoon season (June–September; Xu et  
150 al., 2009), respectively. Thus, we conduct analyses according to different altitudes (above or below  
151 5200 m a.s.l.) and seasons (monsoon or non-monsoon). In addition, for any observational site with  
152 multiple measurements during the same season, we average the measurements to represent the  
153 mean BC pollution condition for this site during the season. Since a rather limited number of sites  
154 provide vertically resolved BC measurements throughout snowpack, we average BC  
155 concentrations throughout snow layers at these sites, which may introduce some uncertainties.

156 Figures 1a–1f show that BC concentrations in snow are generally much higher during the  
157 non-monsoon period than during the monsoon period by up to one order of magnitude, except for

158 NWTP and NOTP. This is because the four sub-regions (NETP, SETP, CTP, and HIMA) are  
159 dominated by the strong BC emissions in the non-monsoon season (particularly winter and spring)  
160 over South and East Asia (Lu et al., 2012; Zhang et al., 2015; Yang et al., 2018) and the efficient  
161 wet removal of BC in Asia in the monsoon season (Xu et al., 2009; He et al., 2014a). In contrast,  
162 the high concentrations during the monsoon period over NWTP and NOTP are primarily caused  
163 by the enrichment of BC via sublimation and/or melting of snow (Ming et al., 2009; Yang et al.,  
164 2015) and emissions from Central Asia and Middle East (Kopacz et al., 2011; Schmale et al., 2017).

165 Furthermore, BC concentrations are consistently larger at low altitudes (<5200 m) than at  
166 high altitudes (>5200 m) by a factor of 2–10 in each sub-region (Figs. 1a–1f), which is consistent  
167 with previous studies (Ming et al., 2009, 2013) which suggested that BC concentrations decrease  
168 with increasing elevations. Such altitudinal contrast in BC concentrations are maximal (with  
169 differences larger than one order of magnitude) over HIMA and SETP. This elevational  
170 dependence can be attributed to the stronger local emissions at lower elevations, the reduced  
171 efficiency of BC transport to higher elevations, and the higher temperature at lower elevations  
172 leading to stronger snow melting and hence BC enrichment in snow (e.g., Ming et al., 2013; Niu  
173 et al., 2017; Zhang et al., 2018).

174 Among the six sub-regions, the high-altitude areas in HIMA and SETP show the lowest  
175 BC concentrations (5–30 ppb) throughout the year (Figs. 1d–1f), while NETP (with only low-  
176 altitude sites) during the non-monsoon season is most severely polluted by BC (~4300 ppb). The  
177 results further indicate that BC concentrations in low-altitude areas across different sub-regions  
178 are comparable (190–450 ppb) during the monsoon season but are much more variable during the  
179 non-monsoon season (Figs. 1d–1f). The variation of BC concentrations across the sub-regions is a  
180 result of combined effects of the aforementioned factors (e.g., regionally and seasonally dependent  
181 impacts from BC source, transport, removal, and snow aging). We note that the current  
182 observations over the TP are still rather limited spatially and temporally, leading to questions of  
183 representativeness and introducing uncertainty in the analysis. Thus, the large sub-regional,  
184 altitudinal, and seasonal heterogeneity of BC concentrations in the TP snowpack highlights an  
185 urgent need for extensive measurements.

186

### 187 **3. Model description, implementation, and evaluation**

#### 188 **3.1 SNICAR model**

189 Flanner et al. (2007) developed a multi-layer SNOW, ICE, and Aerosol Radiative (SNICAR)  
190 model, which has been widely used for snowpack simulations globally. It is also coupled to global  
191 climate models (e.g., Community Earth System Model, CESM) to investigate effects of impurity  
192 contamination, snow grain properties, and snow aging on snowpack albedo. A detailed model  
193 description has been presented by Flanner et al. (2007) and implementation in CESM is described  
194 by Oleson et al. (2013). Here we briefly summarize the key model elements related to the present  
195 study. SNICAR simulates snowpack radiative transfer based on the theory from Wiscombe and  
196 Warren (1980) and the multi-layer two-stream radiative transfer solution from Toon et al. (1989).  
197 It resolves vertical distributions of snow properties, impurity distributions, and heating throughout  
198 the snowpack column, as well as impact of underlying ground surfaces. The number of snow layers  
199 can be specified by users according to research objectives. The default SNICAR model assumes  
200 spherical snow grains and external mixing between impurities and snow grains. As inputs to  
201 radiative transfer calculations, the optical properties (extinction cross section ( $Q_{ext}$ ), single-  
202 scattering albedo ( $\omega$ ), and asymmetry factor ( $g$ )) of snow grains and impurities, archived as lookup  
203 tables, are offline computed by the Mie theory based on particle size distributions and refractive  
204 indices. SNICAR utilizes clear- and cloudy-sky surface incident solar flux typical of mid-latitude  
205 winter. The input parameters for SNICAR include incident radiation type (direct/diffuse), solar  
206 zenith angle, number of snow layers with thickness, density, and grain effective radius in each  
207 layer, underlying ground albedo, and aerosol concentrations in snow. In this study, we use the  
208 stand-alone version of SNICAR (available at <http://snow.engin.umich.edu/snicarcode/>) and  
209 implement new parameterizations of snow nonsphericity and BC-snow internal mixing into it (see  
210 Sections 3.2 and 3.3). The updated SNICAR model is available at  
211 <https://github.com/EarthSciCode/SNICARv2>.

212

### 213 3.2 Implementation of nonspherical snow grains

214 Previous studies commonly used an effective spherical snow grain with an equal volume-  
215 to-area ratio (i.e., equal surface area-weighted mean radius; hereinafter effective radius,  $R_e$ ) to  
216 represent its nonspherical counterpart (e.g., Fu et al., 1999; Grenfell et al., 2005). The equal-  
217 effective-radius representation works well in computing extinction efficiency and single-scattering  
218 albedo but is inaccurate for asymmetry factor (Dang et al., 2016). To explicitly resolve snow grain  
219 shapes, Liou et al. (2014) have developed a stochastic snow albedo model based on a geometric-

220 optics surface-wave (GOS) approach (Liou et al., 2011; He et al., 2015, 2016; Liou and Yang,  
 221 2016). Further, He et al. (2017b) developed a parameterization to account for snow nonsphericity  
 222 effects on asymmetry factors for three typical grain shapes, including spheroid, hexagonal plate,  
 223 and Koch snowflake (see Fig. 1 of He et al. 2017b). They parameterized the asymmetry factor ( $g_{ns}$ )  
 224 of nonspherical snow grains as follows:

$$225 \quad g_{ns} = g_{hex} \times C_g \quad (1)$$

$$226 \quad C_g = a_0 \left( \frac{f_{s,x}}{f_{s,hex}} \right)^{a_1} (2R_s)^{a_2} \quad (2)$$

227 where  $a_i$  ( $i = 0-2$ ) is the wavelength-dependent coefficient available in He et al. (2017b).  $R_s$  (unit:  
 228  $\mu\text{m}$ ) is equal to the snow effective radius ( $R_e$ ) for spheroid or hexagonal plate, and  $R_e/0.544$  for  
 229 Koch snowflake due to its complex concave shape.  $f_{s,x}$  and  $f_{s,hex}$  are the shape factors (i.e., ratio  
 230 of  $R_s$  of a nonspherical grain to that of an equal-volume sphere) of a nonspherical grain ( $x$ : spheroid,  
 231 hexagonal plate, or Koch snowflake) and hexagonal plate, respectively.  $C_g$  is the correction factor,  
 232 and  $g_{hex}$  is the asymmetry factor for hexagonal shapes computed as follows (Fu, 2007):

$$233 \quad g_{hex} = \frac{1-g'}{2\omega} + g' \quad (3)$$

$$234 \quad g' = b_0 + b_1 \times AR + b_2 \times AR^2, \quad \text{for } 0.1 \leq AR \leq 1.0 \quad (4a)$$

$$235 \quad g' = c_0 + c_1 \times \ln(AR) + c_2 \times \ln^2(AR), \quad \text{for } 1.0 < AR \leq 20 \quad (4b)$$

236 where  $\omega$  is the snow single-scattering albedo, and  $g'$  is the asymmetry factor related to geometric  
 237 reflection and refraction.  $b_i$  and  $c_i$  ( $i = 0-2$ ) are the wavelength-dependent coefficients available in  
 238 Fu (2007).  $AR$  is the snow aspect ratio (i.e., ratio of grain width to length).

239 Here we implement the He et al. (2017b) parameterization (Equations 1–4) for snow  
 240 asymmetry factor into SNICAR to account for nonspherical shapes. Due to the coarse spectral  
 241 resolution (6 bands) of the parameterization, we further use a piece-wise shape-preserved  
 242 polynomial interpolation method (Fritsch and Carlson, 1980) to interpolate the parameterized  
 243 results into 470 bands (0.3–5  $\mu\text{m}$  with a 10-nm resolution) used in SNICAR. The same  
 244 interpolation method is also applied to implementing the single-scattering co-albedo  
 245 parameterization for BC-contaminated snow (see Section 3.3). We use the extinction efficiency  
 246 and single-scattering albedo of equal-effective-radii spheres for those of the nonspherical grains.

247 Figures 2a–2c show the spectral snow asymmetry factors for different grain shapes based  
 248 on the updated SNICAR model. Compared with spherical snow grains, nonspherical grains

249 (particularly Koch snowflakes) result in up to ~17% smaller asymmetry factors at wavelengths <  
250 ~3.0  $\mu\text{m}$ , consistent with previous studies (Liou et al., 2014; Dang et al., 2016). We note that the  
251 results slightly (<3%) overestimate the asymmetry factors at two spectral peaks within 1.5–2.5  $\mu\text{m}$   
252 for spheroids with large sizes ( $R_e \geq 500 \mu\text{m}$ ), due to parameterization uncertainties (He et al.,  
253 2017b).

254 As a result of the smaller asymmetry factors, nonspherical snow grains lead to weaker  
255 forward scattering and hence higher albedo relative to their spherical counterparts (Figs. 3 and S1).  
256 We find up to about 2% and 27% higher albedo for Koch snowflakes in the visible (0.3–0.7  $\mu\text{m}$ )  
257 and near-infrared (NIR, 0.7–5  $\mu\text{m}$ ) bands, respectively, compared to equal- $R_e$  spheres (Figs. 3d  
258 and 3e). These results show good agreement with the conclusions from previous studies (Wang et  
259 al., 2017; He et al., 2018a). The results also have important implications for snow grain size  
260 retrievals via the use of albedo models to match observed spectral reflectance. For example, Dang  
261 et al. (2016) and He et al. (2018a) suggested that if a nonspherical grain is simulated as a sphere,  
262 its effective size has to be scaled down by a factor of 1.2–2.5 to obtain the correct snow albedo.  
263

### 264 3.3 Implementation of BC-snow internal mixing

265 Flanner et al. (2012) showed that the effect of BC-snow internal mixing can be equivalent  
266 to applying an enhancement ratio to BC absorption cross sections with the external mixing  
267 assumption and developed a lookup table for the enhancement ratio. Recently, He et al. (2017b)  
268 explicitly resolved the structures of BC-snow internal mixtures for different snow shapes and  
269 found that inclusions of BC increase snow single-scattering co-albedo ( $1-\omega$ ) and hence absorption  
270 but have negligible effects on snow asymmetry factor and extinction efficiency. They further  
271 parameterized the effect of internal mixing on  $1-\omega$  as follows:

$$272 E_{1-\omega} = d_0 \times (C_{BC} + d_2)^{d_1} \quad (5)$$

273 where  $E_{1-\omega}$  is the co-albedo enhancement defined as the ratio of single-scattering co-albedo for  
274 BC-contaminated snow to that for pure snow, which is a function of BC mass concentration in  
275 snow ( $C_{BC}$ , unit: ppb).  $d_i$  ( $i = 0-2$ ) is the wavelength-dependent parameterization coefficient  
276 available in He et al. (2017b).

277 Here we implement the He et al. (2017b) parameterization (Equation 5) for snow single-  
278 scattering co-albedo to account for BC-snow internal mixing. We note that the BC mass absorption  
279 cross section (MAC) at 550 nm used in He et al. (2017b) is  $6.8 \text{ m}^2 \text{ g}^{-1}$  with a BC density of 1.7 g

280  $\text{cm}^{-3}$  and an effective radius of 0.1  $\mu\text{m}$ . Thus, to obtain a BC MAC of 7.5  $\text{m}^2 \text{g}^{-1}$  at 550 nm  
 281 recommended by Bond and Bergstrom (2006), we adjust the BC size and density in this study. We  
 282 assume a lognormal BC size distribution with a geometric mean diameter of 0.06  $\mu\text{m}$  following  
 283 Dentener et al. (2006) and Yu and Luo (2009) and a geometric standard deviation of 1.5 following  
 284 Flanner et al. (2007) and Aoki et al. (2011). Then, we tune the BC density to 1.49  $\text{g cm}^{-3}$  to match  
 285 the MAC (7.5  $\text{m}^2 \text{g}^{-1}$ ). The resulting BC size effect on  $E_{1-\omega}$  is quantified using a parameterization  
 286 developed by He et al. (2018b) as follows:

$$287 \quad E_{1-\omega, R_{BC}} = k_{\lambda, R_{BC}} \times E_{1-\omega, R_{BC}=0.05}^{f_{\lambda, R_{BC}}} \quad (6a)$$

$$288 \quad \text{with } d_{\lambda, R_{BC}} = \left(\frac{R_{BC}}{0.05}\right)^{m_{\lambda}}, \quad f_{\lambda, R_{BC}} = \left(\frac{R_{BC}}{0.05}\right)^{n_{\lambda}} \quad (6b)$$

289 where  $E_{1-\omega, R_{BC}}$  and  $E_{1-\omega, R_{BC}=0.05}$  are the  $E_{1-\omega}$  for a certain BC effective radius ( $R_{BC}$ ) and a  $R_{BC}$  of  
 290 0.05  $\mu\text{m}$  (reference case), respectively.  $k_{\lambda, R_{BC}}$  and  $f_{\lambda, R_{BC}}$  are empirical parameters relying on  
 291 wavelength and BC size.  $m_{\lambda}$  and  $n_{\lambda}$  are wavelength-dependent coefficients available in He et al.  
 292 (2018b). We should note that BC MAC could vary significantly in reality (e.g., from 2 to 15  $\text{m}^2 \text{g}^{-1}$  at 550 nm) due to uncertainties from particle density, size, structure, and refractive index (Bond and Bergstrom, 2006). Thus, we use the recommended value (7.5  $\text{m}^2 \text{g}^{-1}$ ) derived from a comprehensive review of measurements to reduce the potential uncertainty from BC MAC in this study. Compared with the current estimates, using a smaller BC MAC (e.g., 6.8  $\text{m}^2 \text{g}^{-1}$  at 550 nm as used in He et al. 2017b) would lead to weaker BC-induced snow albedo reductions, the quantification of which, however, is beyond the scope of this study and will be investigated in future work. In addition, the adjusted BC density and size used in the present study are still within the observed ranges, with 1.2–1.9  $\text{g cm}^{-3}$  for densities (Bond and Bergstrom, 2006; Long et al., 2013) as well as 0.01–0.15  $\mu\text{m}$  and 1.2–2.0 for geometric mean diameters and standard deviations (Bond et al., 2006), respectively.

303 Figures 2d–2f show the spectral single-scattering co-albedo of snow internally mixed with  
 304 BC based on the updated SNICAR model. The strongest co-albedo enhancement (up to about 4  
 305 orders of magnitude for 1000 ppb BC) is in the visible band, with negligible effects at  
 306 wavelengths  $>1 \mu\text{m}$ . As a result of the enhanced snow absorption, snow albedo reduces about two-  
 307 fold more due to internal mixing than external mixing (Figs. 4 and S2–S4). In contrast, BC  
 308 decreases snow albedo much less for nonspherical snow grains than spherical grains (Figs. 4 and  
 309 S3–S4), suggesting an important interactive effects of snow grain shape and BC-snow mixing state

Formatted: Font color: Text 1

Formatted: Font color: Text 1

Formatted: Font color: Text 1

310 on snow albedo reductions. For example, BC-sphere external mixing leads to similar visible albedo  
311 reductions with BC-hexagonal plate internal mixing. This is consistent with our previous findings  
312 (He et al., 2018a). Although the internal mixing effect dominates at the NIR wavelengths (Fig. 4e),  
313 the NIR albedo reduction is a factor of 3–5 lower than the visible reduction. Thus, both snow  
314 nonsphericity and BC-snow internal mixing play comparably important roles in determining all-  
315 wavelength albedo reductions (Fig. 4f). This highlights the significance of simultaneously  
316 accounting for these two factors in accurate estimates of BC-snow albedo effects.

317 Moreover, to cross-validate model results, we compare the simulated snow albedo and its  
318 reduction for BC-snow internal mixing using the He et al. (2017b) parameterization with those  
319 using the Flanner et al. (2012) lookup table. We find very good agreement (mean differences <  
320 3%) between the two schemes for different snow sizes and shapes (Figs. 5 and S5–S6), although  
321 the He et al. (2017b) parameterization leads to slightly stronger and weaker albedo reductions for  
322 higher (>1000 ppb) and lower (<1000 ppb) BC concentrations, respectively. Compared with the  
323 lookup table method, the newly-implemented parameterization in this study can be applied to a  
324 wider range of snow grain size, shape, and BC concentration scenarios without sacrificing  
325 computational efficiency.

326

### 327 3.4 Comparisons with observations

#### 328 3.4.1 Pure snow albedo

329 We evaluated spectral pure snow albedo from SNICAR simulations by comparing with  
330 observations (Fig. 6) from laboratory measurements (Hadley and Kirchstetter, 2012), open-field  
331 experiments (Brandt et al., 2011), and field measurements in the Rocky Mountains (Painter et al.,  
332 2007) and at the South Pole (Grenfell et al., 1994). To conduct reasonable comparisons, we used  
333 the observed snow density, grain size, thickness, snowpack layer, direct/diffuse radiation, solar  
334 zenith angle, and underlying ground albedo in model simulations for each case (see Table 1 and  
335 Figure 6 for details), except for underlying ground albedos in the Brandt et al. (2011) and Painter  
336 et al. (2007) cases and the grain size of the second snow layer in the Brandt et al. (2011) case  
337 because of unavailable measurements. Thus, we assumed black underlying grounds (albedo = 0)  
338 in the two cases, which has negligible effects on albedo estimates due to thick snow optical depths.  
339 In the Brandt et al. (2011) case, we further assumed an effective radius of 500  $\mu\text{m}$  (typical for aged  
340 snow) in the second snow layer to make it optically semi-infinite, which is consistent with the

Deleted: snowpack conditions

Deleted: (e.g., snow density, grain size, thickness, snowpack layers, direct/diffuse light, solar zenith angle, and underlying ground albedo)

Deleted: snow

346 ~~observed condition.~~ We also assumed four types of snow shapes (sphere, spheroid, hexagonal plate,  
347 and Koch snowflake) in the simulations to investigate shape effects, due to the lack of  
348 measurements.

349 We find that model simulations generally capture the observed patterns of spectral snow  
350 albedo in all cases (Fig. 6). However, assuming spherical grains tends to underestimate snow  
351 albedo in the NIR band, while using nonspherical grains improves model results. For example,  
352 compared with the observations (Painter et al., 2007), simulations assuming snow spheres show a  
353 systematic underestimate of up to  $\sim 0.1$  at wavelengths  $> 0.7 \mu\text{m}$ , particularly at  $1.0\text{--}1.2 \mu\text{m}$  (Fig.  
354 6c), while simulations assuming hexagonal plates well match the observations. Similarly, in the  
355 observational case of Grenfell et al. (1994), assuming hexagonal plates and Koch snowflakes  
356 substantially reduces model underestimates at  $1.5\text{--}2.5 \mu\text{m}$  relative to assuming spheres, though  
357 leading to a slight overestimate at  $0.9\text{--}1.3 \mu\text{m}$  (Fig. 6d). In contrast, in comparison with the  
358 laboratory measurements from Hadley and Kirchstetter (2012), the spherical assumption works  
359 reasonably well, particularly for large sizes, with only slight ( $< 0.05$ ) underestimates. This is  
360 because the snow grains created in those experiments tend to be spherical. Nevertheless, using  
361 spheroids and hexagonal plates in this case still leads to slightly better model results for large ( $R_e$   
362 =  $65$  and  $110 \mu\text{m}$ ) and small ( $R_e = 55 \mu\text{m}$ ) grain sizes, respectively (Fig. 6a). In the observational  
363 case of Brandt et al. (2011), they determined snow effective sizes by matching model results with  
364 the measured NIR ( $1.0\text{--}1.3 \mu\text{m}$ ) albedo. We find that assuming different snow shapes results in  
365 drastically different grain sizes retrieved by matching their measured NIR albedo (Figs. 6b and  
366 7d), with effective radii of  $80$  and  $160 \mu\text{m}$  for spheres and Koch snowflakes, respectively. This  
367 implies the necessity of accounting for realistic grain shapes in snow grain size retrievals.

368 We note that model results in all cases show slight but consistent albedo overestimates  
369 around  $400 \text{ nm}$  compared with observations (Fig. 6), probably due to the uncertainty of ice  
370 refractive indices. In this work, we used ice refractive indices from the most widely-used database  
371 (Warren and Brandt, 2008) obtained from measurements in the Antarctic, which shows a very low  
372 ice absorption coefficient around  $400 \text{ nm}$ . However, based on more recent measurements in  
373 Antarctic snow, Picard et al. (2016) found a much higher ice absorption coefficient around  $400 \text{ nm}$   
374 than that from Warren and Brandt (2008), which suggested that the uncertainty in ice visible  
375 absorption is probably larger than generally appreciated. Therefore, the weak snow absorption

Deleted: and made reasonable assumptions for cases when measurements are absent (see Table 1 and Figure 6).

Deleted: further

379 [caused by refractive indices used in this study could lead to the overestimates in modeled albedo](#)  
380 [around 400 nm.](#)

381

### 382 3.4.2 BC-contaminated snow albedo

383 We further compared BC-contaminated snow albedo from SNICAR simulations with  
384 observations (Fig. 7) from laboratory measurements (Hadley and Kirchstetter, 2012), open-field  
385 experiments (Brandt et al., 2011; Svensson et al., 2016), and field measurements in the Arctic  
386 (Meinander et al., 2013; Pedersen et al., 2015). Similar to Section 3.4.1, we used the observed [BC](#)  
387 [concentration in snow, snow density, grain size, thickness, snowpack layer, direct/diffuse radiation,](#)  
388 [solar zenith angle, and underlying ground albedo in model simulations for each case](#) (see Table 1  
389 and Figure 7 for details), [except for the snow density in the Pedersen et al. \(2015\) case and the](#)  
390 [underlying ground albedo in the Meinander et al. \(2013\) case because of unavailable](#)  
391 [measurements. Thus, we assumed a typical fresh snow density of 150 kg m<sup>-3</sup> in the former case](#)  
392 [and a black underlying ground \(albedo = 0\) in the latter case. Compared with assuming a black](#)  
393 [underlying ground, we find that using a non-black underlying ground albedo typically observed](#)  
394 [over the Tibet \(Qu et al., 2014\) only leads to very small \(<5%\) relative differences in albedo](#)  
395 [calculations in the Meinander et al. \(2013\) case.](#) Due to the lack of measurements, we further  
396 assumed BC internally or externally mixed with different snow shapes in the simulations to  
397 quantify the combined effects of BC-snow mixing state and snow grain shape.

398 Compared with the widely-used assumption of BC externally mixed with spherical snow  
399 grains, we find that accounting for both internal mixing and snow nonsphericity improves model  
400 simulations (Fig. 7). For example, assuming BC-sphere external mixing leads to a systematical  
401 underestimate of polluted snow albedo for <2000 ppb BC compared with the observations from  
402 Svensson et al. (2016), while assuming BC-Koch snowflake internal mixing reduces the model  
403 underestimate (Fig. 7b), with the normalized mean bias (NMB) and root-mean-square error  
404 (RMSE) decreasing from -0.04 to 0.01 and from 0.033 to 0.019, respectively. Similarly, in the  
405 observational case of Pedersen et al. (2015), simulations assuming BC-spheroid external mixing  
406 perform better than those assuming BC-sphere external mixing (Fig. 7a), reducing the NMB from  
407 -0.012 to -0.003 and RMSE from 0.028 to 0.025. Compared with the observations of Meinander  
408 et al. (2013), model results using spherical snow grains underestimate the spectral snow albedo  
409 contaminated by BC (Fig. 7c), regardless of model assumptions of BC-snow mixing state. Using

**Deleted:** snowpack conditions in model simulations and made proper assumptions for cases when measurements are absent

**Deleted:** to make reasonable comparisons

**Formatted:** Font color: Text 1

414 nonspherical grains instead increases the simulated albedo and reduces model biases in this case,  
415 although it is still unable to fully capture the observed pattern (Fig. 7c). Considering that snow  
416 grains tend to be spherical in the observations from Hadley and Kirchstetter (2012), we assumed  
417 BC-sphere external/internal mixing in the comparisons. The model results with external mixing  
418 are systematically biased high, particularly for large BC concentrations (>110 ppb), while using  
419 internal mixing effectively reduces the albedo overestimates (Fig. 7e). As such, the observations  
420 fall between the results of external and internal mixing, suggesting a combination of partial  
421 external and internal mixing would best match the observations. Compared with the way of  
422 increasing BC MAC for BC-snow external mixing to reduce model overestimates in polluted snow  
423 albedo, which was used in Hadley and Kirchstetter (2012), the present study provides a physically-  
424 based alternative (i.e., internal mixing) for model improvements. In fact, it is very likely that a  
425 large portion of BC is internally mixed with snow grains in the experiments of Hadley and  
426 Kirchstetter (2012), since they produced the BC-contaminated snow via freezing of aqueous  
427 hydrophilic BC suspensions.

428 We note that the snow grain sizes reported by the aforementioned field studies are retrieved  
429 by different methods, including matching snow model results with measured albedo spectra  
430 (Painter et al., 2007; Hadley and Kirchstetter, 2012; Pedersen et al., 2015) and visual estimates  
431 with tools (Grenfell et al., 1994; Meinander et al., 2013; Svensson et al., 2016) that are not  
432 equivalent to the snow effective size (i.e., surface area-weighted mean radius) defined in SNICAR.  
433 This could introduce uncertainties to snow albedo calculations and model-observation  
434 comparisons.

Formatted: Font color: Text 1

435  
436 **4. BC-snow albedo effects and uncertainties over the Tibetan Plateau**

Deleted: ¶

437 Based on the observed BC concentrations in snow (see Section 2), we applied the updated  
438 SNICAR model (see Section 3) to quantify the present-day (2000–2015) BC-snow albedo  
439 reduction and associated surface radiative effects over the TP. We conducted albedo simulations  
440 at each observational site using the measured snowpack thickness and density (see Table S1)  
441 concurrently with BC measurements. If the snow property measurements are missing at certain  
442 site, the data from nearby sites are used instead. We then computed the regional mean values by  
443 averaging across all sites within each sub-region and season. We used typical effective radii of 100  
444  $\mu\text{m}$  and 1000  $\mu\text{m}$  for fresh and aged snow, respectively, to demonstrate snow aging/size effects.

446 Due to the lack of measurements for snow grain shape and BC-snow mixing state, we considered  
447 eight simulation scenarios with the combination of four snow shapes (sphere, spheroid, hexagonal  
448 plate, and Koch snowflake) and two mixing states (internal and external). In the simulations, the  
449 underlying ground albedo over the TP is 0.1 at the visible band (0.3–0.7  $\mu\text{m}$ ) and 0.2 at the NIR  
450 band (0.7–5  $\mu\text{m}$ ), following observations (Qu et al., 2014). We adopted a solar zenith cosine of  
451 0.65 (i.e., an angle of  $49.5^\circ$ ), which is equivalent to the insolation-weighted solar zenith cosine in  
452 the sunlit hemisphere. The effect of solar zenith angle on snow albedo can be approximated via  
453 changing snow effective size (Marshall, 1989). Previous studies (e.g., Aoki et al., 2003; Dang et  
454 al., 2016) indicated that the impact of snow shape and BC contamination decreases with an  
455 increasing solar zenith angle. Following Dang et al. (2017), we compute all-sky snow albedo via  
456 averages of clear- and cloudy-sky albedo weighted by cloud cover fraction. The mean cloud cover  
457 fraction and all-sky surface downward solar radiation in different sub-regions and seasons (see  
458 Table S2) are derived from the multi-year (2000–2015) monthly mean Modern-Era Retrospective  
459 analysis for Research and Applications version 2 (MERRA-2) reanalysis meteorological fields  
460 (<https://gmao.gsfc.nasa.gov/reanalysis/MERRA-2/>) with a spatial resolution of  $0.5^\circ \times 0.625^\circ$ .

461 Figures 8a–8c show the regional mean BC-induced snow albedo reductions in different  
462 sub-regions and seasons. The spatiotemporal distribution of albedo reductions generally follows  
463 that of BC concentrations in snow (Figs. 1d–1f), with stronger albedo reductions in low-altitude  
464 areas and the non-monsoon period. We find that snow albedo decreases by a factor of 2–3 more  
465 for aged snow (Table S3) than for fresh snow (Table 2), due to larger grain sizes for aged snow.  
466 This aging/size effect dominates the albedo reductions in most of TP sub-regions, particularly  
467 during the monsoon season (Figs. 8a–8c). However, in severely polluted sub-regions including the  
468 low-altitude areas of NETP, SETP, CTP, and HIMA during the non-monsoon season, the effects  
469 of snow grain shape and BC-snow mixing state are comparable to those of snow size/aging (Tables  
470 2 and S3). For example, BC-sphere internal mixing leads to an albedo reduction of 0.114 for fresh  
471 snow in low-altitude CTP during the non-monsoon season, while BC-Koch snowflake external  
472 mixing leads to a reduction of 0.119 for aged snow.

473 Moreover, BC-snow internal mixing enhances the mean albedo reductions by 30–60%  
474 (relative difference) across all the sub-regions and seasons, with similar enhancements for different  
475 snow shapes and sizes (Tables 2 and S3). For example, assuming BC-sphere external mixing leads  
476 to an annual albedo reduction of 0.066 (0.164) for fresh (aged) snow in NETP, while the internal

477 mixing counterpart results in a reduction of 0.095 (0.225). Our results are partially different from  
478 those in He et al. (2018a) which showed a stronger enhancement (relative difference) in albedo  
479 reduction caused by internal mixing for nonspherical grains than spherical grains, due to different  
480 environmental conditions and snow albedo models used in the two studies. We further find that  
481 nonspherical snow grains weaken the mean albedo reductions by up to 31% relative to spherical  
482 grains in different sub-regions and seasons, with the strongest weakening for Koch snowflakes  
483 (Figs. 8a–8c). The nonsphericity effect is smaller for aged snow compared with fresh snow (Tables  
484 2 and S3), consistent with our previous findings (He et al., 2018a).

485 Although the BC concentrations in the TP snowpack tend to dominate the regional and  
486 seasonal pattern of snow albedo reductions for fresh/aged snow (Figs. 1d–1f and 8a–8c), the  
487 combined effects of snow grain shape and BC-snow mixing state can complicate the picture. For  
488 example, with the widely used assumption of BC externally mixed with snow spheres, the non-  
489 monsoon albedo reductions are 0.034 and 0.067 for high-altitude CTP and low-altitude SETP with  
490 BC concentrations of 332 and 1111 ppb in fresh snow, respectively. However, if BC particles were  
491 internally mixed with snow spheres in CTP and externally mixed with Koch snowflakes in SETP,  
492 the albedo reductions in the two areas would become the same (0.047), regardless of the  
493 substantially different BC concentrations. This points toward an imperative need for both extensive  
494 measurements and improved model characterization of snow grain shape and aerosol-snow mixing  
495 state for accurate quantification of BC-induced snow albedo reductions over the TP and elsewhere  
496 with strong heterogeneity of snowpack properties and contamination.

497 Figures 8d–8f show the regional mean surface radiative effects caused by BC-induced  
498 snow albedo reductions, which vary from 0.7 to 11.2 W m<sup>-2</sup> across different sub-regions during  
499 the monsoon season and from 1.2 to 30.7 W m<sup>-2</sup> during the non-monsoon season for BC externally  
500 mixed with fresh snow spheres. The sub-regional variation increases to 1.4–37.7 W m<sup>-2</sup> and 3.5–  
501 58.4 W m<sup>-2</sup> for aged snow during the monsoon and non-monsoon periods, respectively (Tables 3  
502 and S4). In general, the spatiotemporal distribution of surface radiative effects follows that of snow  
503 albedo reductions (Figs. 8a–8f). The impacts of snow nonsphericity and BC-snow internal mixing  
504 on the surface radiative effects are similar to those on the albedo reductions discussed above. The  
505 maximum surface radiative effect over the TP can reach up to 45.4 (79.9) W m<sup>-2</sup> in NETP during  
506 the non-monsoon season for BC internally mixed with fresh (aged) snow spheres (Tables 3 and  
507 S4). The mean BC-induced snow albedo effects in the relatively clean TP areas (e.g., high-altitude

508 HIMA and SETP) are comparable to those over the Arctic and North American snowpack (Dang  
509 et al., 2017; He et al., 2018a), while the effects in the contaminated TP areas (e.g., low-altitude  
510 HIMA, CTP, SETP, and NETP) are generally similar to those in the low-elevation Alps (Painter  
511 et al., 2013) and northern China snowpack (Wang et al., 2017).

512 Previous studies have shown accelerated snowmelt caused by BC-snow albedo effects in  
513 the TP. For example, Yasunari et al. (2010) estimated that BC-induced albedo reductions over  
514 Himalayan glaciers could result in an extra snowmelt of 1–7 mm day<sup>-1</sup> during the melting/summer  
515 season. Qian et al. (2011) found a BC-induced snowmelt of up to 1.3 mm day<sup>-1</sup> in late spring and  
516 early summer averaged over the entire TP. Our results further suggest that the uncertainty  
517 associated with snow shape and BC-snow mixing state could lead to a substantial variation in BC-  
518 induced albedo reduction and hence snowmelt, which has significant implications for runoff and  
519 water management in Asia. Accurate quantifications of the impact of snow grain shape and BC-  
520 snow mixing state on snowmelt and subsequent hydrological processes require interactive land  
521 surface and/or climate modeling, which will be investigated in future work.

522 We note that the present estimates of BC-induced snow albedo effects have uncertainties  
523 and limitations. For example, different techniques have been used to measure BC concentration in  
524 snow/ice, which may lead to discrepancies and inconsistency among observations and in model-  
525 observation comparisons (Qian et al., 2015 and references therein). Besides, BC measurements  
526 across the TP are from various sample types, such as surfaces of snowpack (with fresh/aged snow)  
527 and glacier (with both snow/firn and granular ice), which may introduce uncertainty to the  
528 understanding of BC contamination patterns (Zhang et al., 2017a; Li et al., 2018). In addition, in  
529 the model, we do not account for the vertical variability of BC and snow grain properties in the TP  
530 snowpack as well as some complex snowpack processes, including dynamic snow aging and  
531 melting, post-depositional enrichment, and melting water scavenging, which may exert nontrivial  
532 effects on BC-snow albedo effects (e.g., Flanner et al., 2007; Qian et al., 2014; Dang et al., 2017).

533 These uncertainties associated with modeling and measurements may decrease the signal-to-noise  
534 ratio for the detection of BC effects on snow albedo, particularly in relatively clean regions with  
535 small BC-induced albedo reductions (e.g., <0.01). Thus, improved and robust estimates require  
536 both accurate snow albedo modeling and snowpack measurements.

537

## 538 5. Conclusions, implications, and future work

Deleted: I

Deleted: comprehensive climate

Deleted: coupled with the updated SNICAR snow model

Deleted: constrained by observ

Deleted: ed BC and snowpack conditions

544 We implemented a set of new BC-snow parameterizations into SNICAR, a widely used  
545 snow albedo model, to account for the effects of snow nonsphericity and BC-snow internal mixing.  
546 We evaluated model simulations by comparing with observations. We further applied the updated  
547 SNICAR model with a comprehensive set of *in-situ* measurements of BC concentrations in the  
548 Tibetan Plateau (TP) snowpack (glacier) to quantify the present-day BC-induced snow albedo  
549 effects and associated uncertainties from snow grain shape and BC-snow mixing state.

550 Based on the SNICAR model updated with new BC-snow parameterizations, we found that  
551 nonspherical snow grains tend to have higher pure albedos but lower BC-induced albedo  
552 reductions compared with spherical snow grains, while BC-snow internal mixing substantially  
553 enhances albedo reductions relative to external mixing. Compared with observations, model  
554 simulations assuming nonspherical snow grains and BC-snow internal mixing perform better than  
555 those with the common assumption of snow spheres and external mixing. The results suggest an  
556 important interactive effect from snow nonsphericity and internal mixing, and highlight the  
557 necessity of concurrently accounting for the two factors in snow albedo and climate modeling.

558 We further applied the updated SNICAR model with comprehensive *in-situ* observations  
559 of BC concentrations in snow and snowpack properties over the TP to quantify the present-day  
560 (2000–2015) BC-induced snow albedo effects. We found that BC concentrations show distinct  
561 sub-regional and seasonal variations. The concentrations are generally higher in the non-monsoon  
562 season and low-altitudes (<5200 m) than in the monsoon season and high-altitudes (>5200 m),  
563 respectively. The spatiotemporal distributions of snow albedo reductions and surface radiative  
564 effects generally follow that of BC concentrations. As a result, the BC-induced mean albedo effects  
565 vary by up to an order of magnitude across different sub-regions and seasons, with values of 0.7–  
566 30.7 (1.4–58.4) W m<sup>-2</sup> for BC externally mixed with fresh (aged) snow spheres.

567 Moreover, the BC-snow albedo effects over the TP are significantly affected by the  
568 uncertainty in snow grain shape and BC-snow mixing state. We found that BC-snow internal  
569 mixing enhances the mean albedo effects by 30–60% relative to external mixing across different  
570 sub-regions and seasons, while nonspherical snow grains reduce the albedo effects by up to 31%  
571 relative to spherical grains. These effects become comparably important with the snow aging/size  
572 effect over polluted areas. Therefore, the combined effects of snow grain shape and BC-snow  
573 mixing state can complicate the spatiotemporal features of BC-snow albedo effects over the TP,  
574 with significant implications for regional hydrological processes and water management.

Deleted: W

Deleted: leads to much larger

Deleted: The albedo reductions are weaker for nonspherical snow grains than spherical grains

Deleted: .

Deleted: implying

Deleted: . These results are consistent with previous studies (Flanner et al., 2012; Dang et al., 2016; He et al., 2018a)

Deleted: importance

Deleted: snow grain shape and aerosol-snow mixing state

Deleted: ¶  
–Comparisons with clean snow observations showed that model simulations using spherical snow grains generally capture the observed spectral albedo but lead to a systematic underestimate at NIR wavelengths, while assuming nonspherical snow grains improves model results. Further evaluation with observed BC-contaminated snow albedo indicated that model simulations with the combined effects of snow nonsphericity and BC-snow internal mixing perform better than those with the common assumption of BC externally mixed with snow spheres.

Deleted: We collected available

Deleted: /ice

Deleted:

Deleted: during 2000–2015

Deleted: and significant

Deleted: s

Deleted: Among different sub-regions, the high-altitude areas in the Himalayas and southeastern TP show the lowest mean BC concentrations (<30 ppb) throughout the year, while the northeastern TP during the non-monsoon season is most severely polluted by BC (>4000 ppb). The substantial spatiotemporal heterogeneity of BC concentrations in the TP snowpack implies an urgent need for more extensive measurements.

Deleted: sub-regions

611 In summary, this study points toward an imperative need for improved measurements and  
612 model characterization of snow grain shape and aerosol-snow mixing state in order to accurately  
613 estimate BC-snow albedo effects. In future work, we will incorporate the new features of the  
614 updated SNICAR model into land surface and climate models, including CESM-Community Land  
615 Model (CLM) for global modeling and WRF-Noah-MP for regional modeling, to account for the  
616 effects of snow grain shape and aerosol-snow mixing state and to assess the associated  
617 uncertainties and hydrological feedbacks in global/regional climate system.

618  
619  
620

621 **Data availability.** Users can access the data used and produced by this study via the supplementary  
622 materials and the corresponding author without any restrictions. The updated SNICAR model can  
623 be downloaded at <https://github.com/EarthSciCode/SNICARv2>.

624

625 **Author contributions.** CH designed and performed the parameterization implementation and  
626 model simulations. MF offered data and help in developing model codes. FC and MB helped refine  
627 model experiments. SK and JM provided black carbon observations. KNL and YQ gave valuable  
628 comments. CH prepared the manuscript and all co-authors helped improve the manuscript.

629

630 **Competing interests.** The authors declare that they have no conflict of interest.

631

632 **Acknowledgements.** [The authors thank the three reviewers for their constructive comments.](#) C. He  
633 thanks Wenfu Tang and Roy Rasmussen for helpful discussions. C. He was supported by the  
634 NCAR Advanced Study Program (ASP) Fellowship. The National Center for Atmospheric  
635 Research (NCAR) is sponsored by the National Science Foundation (NSF). The State Key  
636 Program of the National Natural Science Foundation of China is under Grant 91537211 and NCAR  
637 Water System. [K. N. Liou was supported by NSF Grant AGS-1660587.](#) The contribution of Y.  
638 Qian in this study was supported as part of the Energy Exascale Earth System Model (E3SM)  
639 project, funded by the U.S. Department of Energy, Office of Science, Office of Biological and  
640 Environmental Research's Earth System Modeling program. The Pacific Northwest National

**Deleted:** ¶

Based on the observed BC concentrations and snowpack properties, we conducted SNICAR simulations to quantify the BC-induced snow albedo reductions and associated surface radiative effects in different sub-regions and seasons. The spatiotemporal distribution of albedo reductions generally follows that of BC concentrations, with stronger albedo reductions in the non-monsoon period and low-altitude areas. We found that the effects of snow grain shape and BC-snow mixing state become comparably important with the snow aging/size effect over severely polluted areas. BC-snow internal mixing enhances the mean snow albedo reductions by 30–60% relative to external mixing across different sub-regions and seasons, while nonspherical snow grains weaken the albedo reductions by up to 31% relative to spherical grains. Therefore, the combined effects of snow grain shape and BC-snow mixing state can complicate the spatiotemporal features of BC-snow albedo reductions over the TP.¶

We found that the BC-induced mean surface radiative effects can vary by up to an order of magnitude across different sub-regions and seasons, showing a similar pattern with the snow albedo reduction, with the effects further modified by snow grain shape and BC-snow mixing state. The maximum effect can reach up to 45.4 (79.9) W m<sup>-2</sup> in the northeastern TP during the non-monsoon season, assuming BC-sphere internal mixing for fresh (aged) snow. The results suggest that the uncertainty associated with snow shape and BC-snow mixing state over the TP could lead to a large variation in BC-induced snowmelt, with significant implications for hydrological processes and water management in Asia.¶

**Deleted:** extensive

**Deleted:** improved

**Deleted:** induced

**Deleted:** over the TP as well as other areas with highly heterogeneous aerosol contamination and snowpack properties

**Formatted:** Font: Not Bold

678 Laboratory (PNNL) is operated for DOE by Battelle Memorial Institute under contract DE-AC06-  
679 76RLO 1830.

680

681

## 682 **References**

683 Aoki, T., Hachikubo, A., and Hori, M.: Effects of snow physical parameters on shortwave broadband albedos.  
684 *J. Geophys. Res.*, 108(D19), 4616, doi:10.1029/2003JD003506, 2003.

685 Aoki, T., K. Kuchiki, M. Niwano, Y. Kodama, M. Hosaka, and T. Tanaka: Physically based snow albedo model  
686 for calculating broadband albedos and the solar heating profile in snowpack for general circulation models,  
687 *J. Geophys. Res.*, 116, D11114, doi:10.1029/2010JD015507, 2011.

688 Brandt, R. E., Warren, S. G., and Clarke, A. D.: A controlled snowmaking experiment testing the relation  
689 between black carbon content and reduction of snow albedo, 116, D08109, doi:10.1029/2010JD015330, 2011.

690 Bond, T. C., and R. W. Bergstrom: Light absorption by carbonaceous particles: An investigative review, *Aerosol*  
691 *Sci. Technol.*, 40, 27–67, 2006.

692 [Bond, T. C., Habib, G., and Bergstrom, R. W.: Limitations in the enhancement of visible light absorption due to](#)  
693 [mixing state. \*J. Geophys. Res.-Atmos.\*, 111, D20211, doi:10.1029/2006jd007315, 2006.](#)

694 Bond, T. C., Doherty, S. J., Fahey, D. W., Forster, P. M., Berntsen, T., DeAngelo, B. J., Flanner, M. G., Ghan,  
695 S., Kärcher, B., Koch, D., Kinne, S., Kondo, Y., Quinn, P. K., Sarofim, M. C., Schultz, M. G., Schulz, M.,  
696 Venkataraman, C., Zhang, H., Zhang, S., Bellouin, N., Guttikunda, S. K., Hopke, P. K., Jacobson, M. Z.,  
697 Kaiser, J. W., Klimont, Z., Lohmann, U., Schwarz, J. P., Shindell, D., Storelvmo, T., Warren, S. G., and  
698 Zender, C. S.: Bounding the role of black carbon in the climate system: A scientific assessment, *J. Geophys.*  
699 *Res.-Atmos.*, 118, 1–173, doi:10.1002/jgrd.50171, 2013.

700 Dang, C., Q. Fu, and S. Warren: Effect of Snow Grain Shape on Snow Albedo, *J. Atmos. Sci.*, 73, 3573–  
701 3583, doi: 10.1175/JAS-D-15-0276.1, 2016.

702 Dang, C., Warren, S. G., Fu, Q., Doherty, S. J., & Sturm, M.: Measurements of light-absorbing particles in snow  
703 across the Arctic, North America, and China: Effects on surface albedo. *Journal of Geophysical Research:*  
704 *Atmospheres*, 122, 10,149–10,168, doi:10.1002/2017JD027070, 2017.

705 Dentener, F., Kinne, S., Bond, T., Boucher, O., Cofala, J., Generoso, S., Ginoux, P., Gong, S., Hoelzemann, J.  
706 J., Ito, A., Marelli, L., Penner, J. E., Putaud, J.-P., Textor, C., Schulz, M., van der Werf, G. R., and Wilson,  
707 J.: Emissions of primary aerosol and precursor gases in the years 2000 and 1750 prescribed data-sets for  
708 AeroCom, *Atmos. Chem. Phys.*, 6, 4321–4344, doi:10.5194/acp-6-4321-2006, 2006.

709 Di Mauro, B., Baccolo, G., Garzonio, R., Giardino, C., Massabò, D., Piazzalunga, A., Rossini, M., and Colombo,  
710 R.: Impact of impurities and cryoconite on the optical properties of the Morteratsch Glacier (Swiss Alps),  
711 *The Cryosphere*, 11, 2393-2409, doi:10.5194/tc-11-2393-2017, 2017.

712 Dominé, F., T. Lauzier, A. Cabanes, L. Legagneux, W. F. Kuhs, K. Techmer, and T. Heinrichs: Snow  
713 metamorphism as revealed by scanning electron microscopy, *Micros. Res. Tech.*, 62, 33–48, 2003.

714 Flanner, M. G., Zender, C. S., Randerson, J. T., and Rasch, P. J.: Present-day climate forcing and response from  
715 black carbon in snow, *J. Geophys. Res.-Atmos.*, 112, D11202, doi:10.1029/2006jd008003, 2007.

716 Flanner, M. G., Zender, C. S., Hess, P. G., Mahowald, N. M., Painter, T. H., Ramanathan, V., and Rasch, P. J.:  
717 Springtime warming and reduced snow cover from carbonaceous particles, *Atmos. Chem. Phys.*, 9, 2481–  
718 2497, doi:10.5194/acp-9-2481-2009, 2009.

719 Flanner, M. G., X. Liu, C. Zhou, J. E. Penner, and C. Jiao: Enhanced solar energy absorption by internally-mixed  
720 black carbon in snow grains, *Atmos. Chem. Phys.*, 12(10), 4699–4721, doi:10.5194/acp-12-4699-2012, 2012.

Formatted: Font: (Asian) Times New Roman, 10.5 pt,  
(Asian) Chinese (China)

721 Flanner, M. G.: Arctic climate sensitivity to local black carbon, *J. Geophys. Res.-Atmos.*, 118, 1840–1851,  
722 doi:10.1002/jgrd.50176, 2013.

723 Fritsch, F. N. and R. E. Carlson: "Monotone Piecewise Cubic Interpolation," *SIAM J. Numerical Analysis*, 17,  
724 238-246, 1980.

725 Fu, Q.: A new parameterization of an asymmetry factor of cirrus clouds for climate models. *Journal of the*  
726 *Atmospheric Sciences*, 64, 4140–4150, doi:10.1175/2007JAS2289.1, 2007.

727 Fu, Q., W. B. Sun, and P. Yang: On modeling of scattering and absorption by nonspherical cirrus ice particles  
728 in thermal infrared wavelengths. *J. Atmos. Sci.*, 56, 2937–2947, doi:10.1175/1520-  
729 0469(1999)056<2937:MOSAAB.2.0.CO;2, 1999.

730 Grenfell, T. C., Warren, S. G., and Mullen, P. C.: Reflection of solar radiation by the Antarctic snow surface at  
731 ultraviolet, visible, and near-infrared wavelengths, *J. Geophys. Res.*, 99, 18 669–18 684, 1994.

732 Grenfell, T. C., S. P. Neshyba, and S. G. Warren: Representation of a nonspherical ice particle by a collection  
733 of independent spheres for scattering and absorption of radiation: 3. Hollow columns and plates. *J. Geophys.*  
734 *Res.*, 110, D17203, doi:10.1029/2005JD005811, 2005.

735 Hadley, O. L. and Kirchstetter, T. W.: Black-carbon reduction of snow albedo, *Nat. Clim. Change*, 2, 437–440,  
736 doi:10.1038/NCLIMATE1433, 2012.

737 Hansen, J., and Nazarenko, L.: Soot climate forcing via snow and ice albedos, *P. Natl. Acad. Sci. USA*, 101,  
738 423–428, doi:10.1073/pnas.2237157100, 2004.

739 He, C., Li, Q. B., Liou, K. N., Zhang, J., Qi, L., Mao, Y., Gao, M., Lu, Z., Streets, D. G., Zhang, Q., Sarin, M.  
740 M., and Ram, K.: A global 3-D CTM evaluation of black carbon in the Tibetan Plateau, *Atmos. Chem. Phys.*,  
741 14, 7091–7112, doi:10.5194/acp-14-7091-2014, 2014a.

742 He, C., Li, Q. B., Liou, K. N., Takano, Y., Gu, Y., Qi, L., Mao, Y. H., and Leung, L. R.: Black carbon radiative  
743 forcing over the Tibetan Plateau, *Geophys. Res. Lett.*, 41, 7806–7813, doi:10.1002/2014gl062191, 2014b.

744 He, C., K. N. Liou, Y. Takano, R. Zhang, M. Levy Zamora, P. Yang, Q. Li, and L. R. Leung: Variation of the  
745 radiative properties during black carbon aging: theoretical and experimental intercomparison, *Atmos. Chem.*  
746 *Phys.*, 15(20), 11967-11980, doi:10.5194/acp-15-11967-2015, 2015.

747 He, C., Y. Takano, K. N. Liou, P. Yang, Q. Li, and D. W. Mackowski: Intercomparison of the GOS approach,  
748 superposition T-matrix method, and laboratory measurements for black carbon optical properties during  
749 aging, *J. Quant. Spectrosc. Radiat. Transfer.*, 184, 287–296, doi:10.1016/j.jqsrt.2016.08.004, 2016.

750 He, C., Y. Takano, and K. N. Liou: Close packing effects on clean and dirty snow albedo and associated climatic  
751 implications, *Geophys. Res. Lett.*, 44, doi:10.1002/2017GL072916, 2017a.

752 He, C., Takano, Y., Liou, K. N., Yang, P., Li, Q., and Chen, F.: Impact of snow grain shape and black carbon-  
753 snow internal mixing on snow optical properties: Parameterizations for climate models. *Journal of Climate*,  
754 30, 10,019–10,036, doi:10.1175/JCLI-D-17-0300.1, 2017b.

755 He, C., Liou, K. N., Takano, Y., Yang, P., Qi, L., and Chen, F.: Impact of grain shape and multiple black carbon  
756 internal mixing on snow albedo: Parameterization and radiative effect analysis. *J. Geophys. Res.-Atmos.*,  
757 123, 1253–1268, doi:10.1002/2017JD027752, 2018a.

758 He, C., Liou, K. N., and Takano, Y.: Resolving size distribution of black carbon internally mixed with snow:  
759 Impact on snow optical properties and albedo. *Geophysical Research Letters*, 45, 2697–2705,  
760 doi:10.1002/2018GL077062, 2018b.

761 Immerzeel, W. W., van Beek, L. P. H., and Bierkens, M. F. P.: Climate Change Will Affect the Asian Water  
762 Towers, *Science*, 328, 1382–1385, doi:10.1126/science.1183188, 2010.

763 Jacobi, H.-W., Lim, S., Ménégos, M., Ginot, P., Laj, P., Bonasoni, P., Stocchi, P., Marinoni, A., and Arnaud, Y.:  
764 Black carbon in snow in the upper Himalayan Khumbu Valley, Nepal: observations and modeling of the  
765 impact on snow albedo, melting, and radiative forcing, *The Cryosphere*, 9, 1685–1699, doi:10.5194/tc-9-  
766 1685-2015, 2015.

Deleted: -

Deleted: -

Deleted: -

Deleted: -

Deleted: -

772 Jacobson, M. Z.: Climate response of fossil fuel and biofuel soot, accounting for soot's feedback to snow and  
773 sea ice albedo and emissivity, *J. Geophys. Res.-Atmos.*, 109, D21201, doi:10.1029/2004jd004945, 2004.

774 Ji, Z., S. Kang, Z. Cong, Q. Zhang, and T. Yao: Simulation of carbonaceous aerosols over the Third Pole and  
775 adjacent regions: distribution, transportation, deposition, and climatic effects, *Climate Dynamics*, 45(9-10),  
776 2831-2846, doi:10.1007/s00382-015-2509-1, 2015.

777 Kang, S., Xu, Y., You, Q., Flühel, W.-A., Pepin, N., and Yao, T.: Review of climate and cryosphere change in  
778 the Tibetan Plateau, *Environ. Res. Lett.*, 5, 015101, doi:10.1088/1748-9326/5/1/015101, 2010.

779 Kopacz, M., Mauzerall, D. L., Wang, J., Leibensperger, E. M., Henze, D. K., and Singh, K.: Origin and radiative  
780 forcing of black carbon transported to the Himalayas and Tibetan Plateau, *Atmos. Chem. Phys.*, 11, 2837-  
781 2852, doi:10.5194/acp-11-2837-2011, 2011.

782 Kokhanovsky, A. A. and Zege, E. P.: Scattering optics of snow, *Appl. Optics*, 43, 1589-1602, 2004.

783 Kokhanovsky, A.: Spectral reflectance of solar light from dirty snow: a simple theoretical model and its  
784 validation. *The Cryosphere*, 7, 1325-1331, doi:10.5194/tc-7-1325-2013, 2013.

785 Lee, W.-L., K. N. Liou, C. He, H.-C. Liang, T.-C. Wang, Q. Li, Z. Liu, and Q. Yue: Impact of absorbing aerosol  
786 deposition on snow albedo reduction over the southern Tibetan plateau based on satellite observations, *Theor.*  
787 *Appl. Climatol.*, 129(3-4), 1373-1382, doi:10.1007/s00704-016-1860-4, 2017.

788 Li, C., Bosch, C., Kang, S., Andersson, A., Chen, P., Zhang, Q., Cong, Z., Chen, B., Qin, D., and Gustafsson,  
789 Ö.: Sources of black carbon to the Himalayan-Tibetan Plateau glaciers, *Nat. Commun.*, 7, 12574,  
790 <https://doi.org/10.1038/ncomms12574>, 2016.

791 Li, X. F., S. Kang, X. He, B. Qu, L. Tripathee, Z. Jing, R. Paudyal, Y. Li, Y. Zhang, F. Yan, G. Li, C. Li. Light-  
792 absorbing impurities accelerate glacier melt in the Central Tibetan Plateau. *Science of the Total Environment*,  
793 587-588: 482-490. Doi: 10.1016/j.scitotenv.2017.02.169, 2017.

794 Li, X., S. Kang, G. Zhang, B. Que, L. Tripathee, R. Paudyal, Z. Jing, Y. Zhang, F. Yan, G. Li, X. Cui, R. Xu,  
795 Z. Hu, C. Li. Light-absorbing impurities in a southern Tibetan Plateau glacier: Variations and potential impact  
796 on snow albedo and radiative forcing. *Atmospheric Research*, 200, 77-87,  
797 doi:10.1016/j.atmosres.2017.10.002, 2018.

798 Liou, K. N., Y. Takano, and P. Yang: Light absorption and scattering by aggregates: Application to black carbon  
799 and snow grains, *J. Quant. Spectrosc. Radiat. Transfer*, 112(10), 1581-1594, doi:10.1016/j.jqsrt.2011.03.007,  
800 2011.

801 Liou, K. N., Y. Takano, C. He, P. Yang, R. L. Leung, Y. Gu, and W. L. Lee: Stochastic parameterization for  
802 light absorption by internally mixed BC/dust in snow grains for application to climate models, *J. Geophys.*  
803 *Res.-Atmos.*, 119, 7616-7632, doi:10.1002/2014JD021665, 2014.

804 Liou, K. N., and P. Yang: *Light Scattering by Ice Crystals: Fundamentals and Applications*, pp. 168-173,  
805 Cambridge Univ. Press, Cambridge, U. K., 2016.

806 [Long, C.M., Nascarella, M.A., Valberg, P.A., 2013. Carbon black vs. black carbon and other airborne materials  
807 containing elemental carbon: physical and chemical distinctions. \*Environ. Pollut.\*, 181, 271-286.](#)

808 Lu, Z. F., Streets, D. G., Zhang, Q., and Wang, S.W.: A novel backtrajectory analysis of the origin of black  
809 carbon transported to the Himalayas and Tibetan Plateau during 1996-2010, *Geophys. Res. Lett.*, 39, L01809,  
810 doi:10.1029/2011gl049903, 2012.

811 Manabe, S. and Terpstra, T. B.: The effects of mountains on the general circulation of the atmosphere as  
812 identified by numerical experiments, *J. Atmos. Sci.*, 31, 3-42, 1974.

813 Marshall, S. E.: *A physical parameterization of snow albedo for use in climate models*, NCAR Cooperative  
814 Thesis 123 (175 pp.), Boulder, CO: National Center for Atmospheric Research, 1989.

815 McConnell, J. R., R. Edwards, G. L. Kok, M. G. Flanner, C. S. Zender, E. S. Saltzman, J. R. Banta, D. R.  
816 Pasteris, M. M. Carter, and J. D. W. Kahl: 20th-century industrial black carbon emissions altered arctic  
817 climate forcing, *Science*, 317, 1381-1384, doi:10.1126/science.1144856, 2007.

Formatted: Font: 10.5 pt

Formatted: Font: 10.5 pt

818 Meinander, O., Kazadzis, S., Arola, A., Riihelä, A., Räisänen, P., Kivi, R., Kontu, A., Kouznetsov, R., Sofiev,  
819 M., Svensson, J., Suokanerva, H., Aaltonen, V., Manninen, T., Roujean, J.-L., and Hautecoeur, O.: Spectral  
820 albedo of seasonal snow during intensive melt period at Sodankylä, beyond the Arctic Circle, *Atmos. Chem.*  
821 *Phys.*, 13, 3793–3810, doi:10.5194/acp-13-3793-2013, 2013.

822 Menon, S., Koch, D., Beig, G., Sahu, S., Fasullo, J., and Orlikowski, D.: Black carbon aerosols and the third  
823 polar ice cap, *Atmos. Chem. Phys.*, 10, 4559–4571, doi:10.5194/acp-10-4559-2010, 2010.

824 Ming, J., Cachier, H., Xiao, C., Qin, D., Kang, S., Hou, S., and Xu, J.: Black carbon record based on a shallow  
825 Himalayan ice core and its climatic implications, *Atmos. Chem. Phys.*, 8, 1343–1352, doi:10.5194/acp-8-  
826 1343-2008, 2008.

827 Ming, J., Xiao, C. D., Cachier, H., Qin, D. H., Qin, X., Li, Z. Q., and Pu, J. C.: Black Carbon (BC) in the snow  
828 of glaciers in west China and its potential effects on albedos, *Atmos. Res.*, 92, 114–123,  
829 doi:10.1016/j.atmosres.2008.09.007, 2009.

830 Ming, J., Xiao, C. D., Du, Z. C., and Yang, X. G.: An overview of black carbon deposition in High Asia glaciers  
831 and its impacts on radiation balance, *Advances in Water Resources*, 55, 80–87,  
832 doi:10.1016/j.advwatres.2012.05.015, 2013.

833 Niu, H.W., S.C. Kang, Y.L. Zhang, X.Y. Shi, X.F. Shi, S.J. Wang, et al.: Distribution of light-absorbing  
834 impurities in snow of glacier on Mt. Yulong, southeastern Tibetan Plateau, *Atmos. Res.*, 197, 474–484,  
835 doi:10.1016/j.atmosres.2017.07.004, 2017.

836 Oleson, K., et al.: Technical description of version 4.5 of the Community Land Model (CLM). NCAR Technical  
837 Note NCAR/TN-503+STR, 420 pp, doi:10.5065/D6RR1W7M, 2013.

838 Painter, T. H., Barrett, A. P., Landry, C. C., Neff, J. C., Cassidy, M. P., Lawrence, C. R., McBride, K. E., and  
839 Farmer, G. L.: Impact of disturbed desert soils on duration of mountain snow cover, *Geophys. Res. Lett.*, 34,  
840 L12502, doi:10.1029/2007GL030284, 2007.

841 Painter, T. H., Flanner, M. G., Kaser, G., Marzeion, B., VanCuren, R. A., and Abdalati, W.: End of the Little Ice  
842 Age in the Alps forced by industrial black carbon, *P. Natl. Acad. Sci. USA*, 110, 15216–15221,  
843 doi:10.1073/pnas.1302570110, 2013.

844 Pedersen, C. A., J.-C. Gallet, J. Ström, S. Gerland, S. R. Hudson, S. Forsström, E. Isaksson, and T. K. Berntsen:  
845 In situ observations of black carbon in snow and the corresponding spectral surface albedo reduction, *J.*  
846 *Geophys. Res. Atmos.*, 120, 1476–1489, doi:10.1002/2014JD022407, 2015.

847 [Picard, G., Libois, Q., and Arnaud, L.: Refinement of the ice absorption spectrum in the visible using radiance  
848 profile measurements in Antarctic snow. \*The Cryosphere\*, 10, 2655–2672. \[https://doi.org/10.5194/tc-10-  
849 2655-2016\]\(https://doi.org/10.5194/tc-10-2655-2016\).](https://doi.org/10.5194/tc-10-2655-2016)

850 Qian, Y., W. I. Gustafson, Jr, LYR Leung, and SJ Ghan: Effects of soot-induced snow albedo change on  
851 snowpack and hydrological cycle in western United States based on Weather Research and Forecasting  
852 chemistry and regional climate simulations, *Journal of Geophysical Research – Atmospheres*, 114, D03108,  
853 doi:10.1029/2008JD011039, 2009.

854 Qian, Y., Flanner, M. G., Leung, L. R., and Wang, W.: Sensitivity studies on the impacts of Tibetan Plateau  
855 snowpack pollution on the Asian hydrological cycle and monsoon climate, *Atmos. Chem. Phys.*, 11, 1929–  
856 1948, doi:10.5194/acp-11-1929-2011, 2011.

857 Qian, Y., H. Wang, R. Zhang, M. G. Flanner, and P. J. Rasch: A Sensitivity Study on Modeling Black Carbon in  
858 Snow and its Radiative Forcing over the Arctic and Northern China, *Environmental Research Letters*, 9(6),  
859 064001, doi:10.1088/1748-9326/9/6/064001, 2014.

860 Qian, Y., Yasunari, T. J., Doherty, S. J., Flanner, M. G., Lau, W. K., Ming, J., Wang, H., Wang, M., Warren, S.  
861 G., and Zhang, R.: Light-absorbing particles in snow and ice: Measurement and modeling of climatic and  
862 hydrological impact, *Adv. Atmos. Sci.*, 32, 64–91, 2015.

Formatted: Font: Times New Roman, 10.5 pt, Font color: Auto, Pattern: Clear

863 Qin, D. H., Liu, S. Y., and Li, P. J.: Snow cover distribution, variability, and response to climate change in  
864 western China, *J. Clim.*, 19(9), 1820–1833, 2006.

865 Qu, B., Ming, J., Kang, S.-C., Zhang, G.-S., Li, Y.-W., Li, C.-D., Zhao, S.-Y., Ji, Z.-M., and Cao, J.-J.: The  
866 decreasing albedo of the Zhadang glacier on western Nyainqentanglha and the role of light-absorbing  
867 impurities, *Atmos. Chem. Phys.*, 14, 11117–11128, doi:10.5194/acp-14-11117-2014, 2014.

868 Qu, X. and A. Hall: Assessing Snow Albedo Feedback in Simulated Climate Change. *J. Climate*, 19, 2617–  
869 2630, doi:10.1175/JCLI3750.1, 2006.

870 Ramanathan, V., and Carmichael, G.: Global and regional climate changes due to black carbon, *Nat. Geosci.*, 1,  
871 221–227, doi:10.1038/Ngeo156, 2008.

872 Räisänen, P., Makkonen, R., Kirkevåg, A., and Debernard, J. B.: Effects of snow grain shape on climate  
873 simulations: sensitivity tests with the Norwegian Earth System Model, *The Cryosphere*, 11, 2919–2942,  
874 doi:10.5194/tc-11-2919-2017, 2017.

875 Schmale, J., Flanner, M., Kang, S., Sprenger, M., Zhang, Q., Guo, J., Li, Y., Schwikowski, M., and Farinotti, D.:  
876 Modulation of snow reflectance and snowmelt from Central Asian glaciers by anthropogenic black carbon,  
877 *Sci. Rep.-UK*, 7, 40501, doi:10.1038/srep40501, 2017.

878 Skiles, S. M. and Painter, T. H.: Daily evolution in dust and black carbon content, snow grain size, and snow  
879 albedo during snowmelt, RockyMountains, Colorado, *J. Glaciol.*, 63, 118–132, doi:10.1017/jog.2016.125,  
880 2016.

881 Sterle, K. M., McConnell, J. R., Dozier, J., Edwards, R., and Flanner, M. G.: Retention and radiative forcing of  
882 black carbon in eastern Sierra Nevada snow, *The Cryosphere*, 7, 365–374, doi:10.5194/tc-7-365-2013, 2013.

883 Svensson J., Virkkula A., Meinander O., Kivekäs N., Hannula H.-R., Järvinen O., Peltoniemi J.I., Gritsevich M.,  
884 Heikkilä A., Kontu A., Neitola K., Brus D., Dagsson-Waldhauserova P., Anttila K., Vehkamäki M., Hienola  
885 A., de Leeuw G., and Lihavainen H.: Soot-doped natural snow and its albedo—results from field experiments.  
886 *Boreal Env. Res.* 21: 481–503, 2016.

887 Toon, O. B., McKay, C. P., Ackerman, T. P., and Santhanam, K.: Rapid calculation of radiative heating rates  
888 and photodissociation rates in inhomogeneous multiple scattering atmospheres, *J. Geophys. Res.*, 94, 16287–  
889 16301, 1989.

890 Wang, M, B Xu, J Cao, X Tie, H Wang, R Zhang, Y Qian, PJ Rasch, S Zhao, G Wu, H Zhao, DR Joswiak, J Li,  
891 and Y Xie: Carbonaceous Aerosols Recorded in a Southeastern Tibetan Glacier: Analysis of Temporal  
892 Variations and Model Estimates of Sources and Radiative Forcing, *Atmos. Chem. Phys.*, 15, 1191–1204,  
893 doi:10.5194/acp-15-1191-2015, 2015.

894 Wang, X., Doherty, S. J., and Huang, J.: Black carbon and other light-absorbing impurities in snow across  
895 northern China, *J. Geophys. Res. Atmos.*, 118, 1471–1492, doi:10.1029/2012JD018291, 2013.

896 Wang, X., Pu, W., Ren, Y., Zhang, X., Zhang, X., Shi, J., Jin, H., Dai, M., and Chen, Q.: Observations and model  
897 simulations of snow albedo reduction in seasonal snow due to insoluble light-absorbing particles during 2014  
898 Chinese survey, *Atmos. Chem. Phys.*, 17, 2279–2296, doi:10.5194/acp-17-2279-2017, 2017.

899 [Warren, S. G., and R. E. Brandt: Optical constants of ice from the ultraviolet to the microwave: A revised  
900 compilation, \*J. Geophys. Res.\*, 113, D14220, doi:10.1029/2007JD009744, 2008.](#)

901 Warren, S. G., and W. J. Wiscombe: A Model for the Spectral Albedo of Snow. 2. Snow Containing Atmospheric  
902 Aerosols, *J. Atmos. Sci.*, 37(12), 2734–2745, 1980.

903 Wiscombe, W. J., and Warren, S. G.: A model for the spectral albedo of snow: I. Pure snow. *Journal of the  
904 Atmospheric Sciences*, 37(12), 2712–2733, doi:10.1175/1520-  
905 0469(1980)037%3C2712:AMFTSA%3E2.0.CO;2, 1980.

906 Wu, L., Gu, Y., Jiang, J. H., Su, H., Yu, N., Zhao, C., Qian, Y., Zhao, B., Liou, K.-N., and Choi, Y.-S.: Impacts  
907 of aerosols on seasonal precipitation and snowpack in California based on convection-permitting WRF-Chem  
908 simulations, *Atmos. Chem. Phys.*, 18, 5529–5547, doi:10.5194/acp-18-5529-2018, 2018.

Formatted: Font: 10.5 pt

Formatted: Font: 10.5 pt

Formatted: Font: 10.5 pt

Formatted: Font: 10.5 pt

Formatted: Font: (Asian) SimSun

909 Xu, B. Q., Cao, J. J., Hansen, J., Yao, T. D., Joswila, D. R., Wang, N. L., Wu, G. J., Wang, M., Zhao, H. B.,  
910 Yang, W., Liu, X. Q., and He, J. Q.: Black soot and the survival of Tibetan glaciers, *P. Natl. Acad. Sci. USA*,  
911 106, 22114–22118, doi:10.1073/pnas.0910444106, 2009.

912 Yang J., S. Kang, Z. Ji, D. Chen. Modeling the origin of anthropogenic black carbon and its climatic effect over  
913 the Tibetan Plateau and surrounding regions. *Journal of Geophysical Research: Atmospheres*, 123. Doi:  
914 10.1002/2017JD027282, 2018.

915 Yang, S., B. Xu, J. Cao, C. S. Zender, and M. Wang: Climate effect of black carbon aerosol in a TP glacier,  
916 *Atmos. Environ.*, 111, 71–78, doi:10.1016/j.atmosenv.2015.03.016, 2015.

917 Yao, T., Thompson, L. G., Mosbrugger, V., Zhang, F., Ma, Y., Luo, T., Xu, B., Yang, X., Joswiak, D. R., Wang,  
918 W., Joswiak, M. E., Devkota, L. P., Tayal, S., Jilani, R., and Fayziev, R.: Third Pole Environment (TPE),  
919 *Environ. Dev.*, 3, 52–64, doi:10.1016/j.envdev.2012.04.002, 2012.

920 Yasunari, T. J., Bonasoni, P., Laj, P., Fujita, K., Vuillermoz, E., Marinoni, A., Cristofanelli, P., Duchi, R., Tartari,  
921 G., and Lau, K. M.: Estimated impact of black carbon deposition during premonsoon season from Nepal  
922 Climate Observatory – Pyramid data and snow albedo changes over Himalayan glaciers, *Atmos. Chem. Phys.*,  
923 10, 6603–6615, doi:10.5194/acp-10-6603-2010, 2010.

924 Yeh, T.-C., Gao, Y. X., Tang, M. C., Luo, S. W., Shen, C. B., Gao, D. Y., Song, Z. S., Qian, Y. F., Yuan, F. M.,  
925 Li, G. Q., Ding, Y. H., Chen, Z. T., Zhou, M. Y., Yang, K. J., and Wang, Q. Q.: Meteorology of Qinhai-  
926 Xizhang (Tibetan) Plateau, Science Press, Beijing, 300 pp., 1979 (in Chinese).

927 Yu, F. and Luo, G.: Simulation of particle size distribution with a global aerosol model: contribution of  
928 nucleation to aerosol and CCN number concentrations, *Atmos. Chem. Phys.*, 9, 7691–7710, doi:10.5194/acp-  
929 9-7691-2009, 2009.

930 Zhao, C., Hu, Z., Qian, Y., Ruby Leung, L., Huang, J., Huang, M., Jin, J., Flanner, M. G., Zhang, R., Wang, H.,  
931 Yan, H., Lu, Z., and Streets, D. G.: Simulating black carbon and dust and their radiative forcing in seasonal  
932 snow: a case study over North China with field campaign measurements, *Atmos. Chem. Phys.*, 14, 11475-  
933 11491, doi:10.5194/acp-14-11475-2014, 2014.

934 Zhang, R., Wang, H., Qian, Y., Rasch, P. J., Easter, R. C., Ma, P.-L., Singh, B., Huang, J., and Fu, Q.:  
935 Quantifying sources, transport, deposition, and radiative forcing of black carbon over the Himalayas and  
936 Tibetan Plateau, *Atmos. Chem. Phys.*, 15, 6205-6223, doi:10.5194/acp-15-6205-2015, 2015.

937 Zhang, Y. L., S. Kang, Z. Cong, J. Schmale, M. Sprenger, C. Li, W. Yang, T. Gao, M. Sillanpää, X. Li, Y. Liu,  
938 P. Chen, X. Zhang. Light-absorbing impurities enhance glacier albedo reduction in the southeastern Tibetan  
939 Plateau. *Journal of Geophysical Research - Atmosphere*, 122. Doi: 10.1002/2016JD026397, 2017a.

940 Zhang, Y. L., S. Kang, C. Li, T. Gao, Z. Cong, M. Sprenger, Y. Liu, X. Li, J. Guo, M. Sillanpää, K. Wang, J.  
941 Chen, Y. Li, S. Sun: Characteristics of black carbon in snow from Laohugou No. 12 glacier on the northern  
942 Tibetan Plateau, *Science of the Total Environment*, 607-608, 1237-1249,  
943 doi:10.1016/j.scitotenv.2017.07.100, 2017b.

944 Zhang, Y., Kang, S., Sprenger, M., Cong, Z., Gao, T., Li, C., Tao, S., Li, X., Zhong, X., Xu, M., Meng, W.,  
945 Neupane, B., Qin, X., and Sillanpää, M.: Black carbon and mineral dust in snow cover on the Tibetan Plateau,  
946 *The Cryosphere*, 12, 413-431, doi:10.5194/tc-12-413-2018, 2018.

Deleted: ¶

947  
948  
949  
950  
951  
952  
953  
954

956 **Table 1.** Parameter values used in SNICAR simulations when comparing with observed snow  
 957 albedo (see Figs. 6 and 7). The observed snowpack properties are used in each case when they are  
 958 available. Four types of snow shapes (sphere, spheroid, hexagonal plate, and Koch snowflake)  
 959 and/or two types of BC-snow mixing (internal and external) are assumed in the simulations.  
 960

Observational cases		Model parameters							
References	Type	Radiation	Solar zenith angle	Underlying ground albedo	Snow layer	Snow thickness (cm)	Snow effective radius (µm)	Snow density (kg m <sup>-3</sup> )	BC content (ppb)
Pure snow									
Hadley and Kirchstetter 2012	laboratory measurement	direct	0°	0	1	semi-infinite	55/65/110	550	
Brandt et al. 2011	open-field experiment	diffuse		0*	2	15 40	80/95/140/160 500*	150 300	0
Painter et al. 2007	field measurement	diffuse		0*	1	100	750	350	Deleted: 600
Grenfell et al. 1994	field measurement	diffuse		0.6	multiple layers with layer-specific properties (see reference for details)				
BC-contaminated snow									
Pedersen et al. 2015	field measurement	diffuse		0.2	1	multiple cases with case-specific properties (see reference for details)		150*	case-specific (see reference for details)
Svensson et al. 2016	open-field experiment	direct	61.3°	0.1	multiple layers with layer-specific snow properties & vertically averaged BC concentrations (see reference for details)				232/489/554/ 1030/6420
Meinander et al. 2013	field measurement	direct	55°	0*	2	0.5 9.5	1000 5000	350 350	87.1
Brandt et al. 2011	open-field experiment	diffuse		0*	2	15 40	80/95/140/160 500*	150 300	2250 20
Hadley and Kirchstetter 2012	laboratory measurement	direct	0°	0	1	semi-infinite	55/65/110	550	110/450/860/ 1680

961 \*The parameters are assumed in simulations due to the lack of measurements. Note that the assumed underlying  
 962 ground albedos have rather small effects on albedo simulations due to thick snow optical depths.

963  
 964  
 965  
 966  
 967  
 968  
 969

971 **Table 2.** Regional and seasonal mean BC-induced all-sky snow albedo reductions for fresh snow  
 972 over the Tibetan Plateau during 2000–2015. See Table S3 for results of aged snow.

Region <sup>1</sup>	Season	BC mean content (ppb)	Fresh snow ( $R_e = 100 \mu\text{m}$ )							
			External mixing				Internal mixing			
			Sphere	Spheroid	Hexagonal plate	Koch snowflake	Sphere	Spheroid	Hexagonal plate	Koch snowflake
HIMA	high alt. monsoon	16.3	$0.5 \times 10^{-2}$	$0.5 \times 10^{-2}$	$0.4 \times 10^{-2}$	$0.4 \times 10^{-2}$	$0.7 \times 10^{-2}$	$0.6 \times 10^{-2}$	$0.5 \times 10^{-2}$	$0.5 \times 10^{-2}$
	low alt. monsoon	29.4	$0.8 \times 10^{-2}$	$0.7 \times 10^{-2}$	$0.6 \times 10^{-2}$	$0.6 \times 10^{-2}$	$1.1 \times 10^{-2}$	$1.0 \times 10^{-2}$	$0.8 \times 10^{-2}$	$0.7 \times 10^{-2}$
	high alt. non-monsoon	1151.8	$6.6 \times 10^{-2}$	$6.1 \times 10^{-2}$	$5.2 \times 10^{-2}$	$4.9 \times 10^{-2}$	$9.8 \times 10^{-2}$	$9.1 \times 10^{-2}$	$7.7 \times 10^{-2}$	$7.2 \times 10^{-2}$
	low alt. non-monsoon	17.5	$0.6 \times 10^{-2}$	$0.5 \times 10^{-2}$	$0.4 \times 10^{-2}$	$0.4 \times 10^{-2}$	$0.8 \times 10^{-2}$	$0.7 \times 10^{-2}$	$0.6 \times 10^{-2}$	$0.5 \times 10^{-2}$
CTP	high alt. monsoon	63.2	$1.4 \times 10^{-2}$	$1.2 \times 10^{-2}$	$1.0 \times 10^{-2}$	$0.9 \times 10^{-2}$	$1.8 \times 10^{-2}$	$1.6 \times 10^{-2}$	$1.4 \times 10^{-2}$	$1.2 \times 10^{-2}$
	low alt. monsoon	446.0	$4.7 \times 10^{-2}$	$4.3 \times 10^{-2}$	$3.6 \times 10^{-2}$	$3.3 \times 10^{-2}$	$6.5 \times 10^{-2}$	$6.0 \times 10^{-2}$	$5.0 \times 10^{-2}$	$4.6 \times 10^{-2}$
	high alt. non-monsoon	331.6	$3.4 \times 10^{-2}$	$3.1 \times 10^{-2}$	$2.6 \times 10^{-2}$	$2.3 \times 10^{-2}$	$4.7 \times 10^{-2}$	$4.3 \times 10^{-2}$	$3.6 \times 10^{-2}$	$3.3 \times 10^{-2}$
	low alt. non-monsoon	1632.9	$7.7 \times 10^{-2}$	$7.1 \times 10^{-2}$	$6.1 \times 10^{-2}$	$5.7 \times 10^{-2}$	$11.4 \times 10^{-2}$	$10.6 \times 10^{-2}$	$9.1 \times 10^{-2}$	$8.4 \times 10^{-2}$
NWTP	high alt. monsoon	143.6	$2.3 \times 10^{-2}$	$2.1 \times 10^{-2}$	$1.7 \times 10^{-2}$	$1.6 \times 10^{-2}$	$3.0 \times 10^{-2}$	$2.7 \times 10^{-2}$	$2.3 \times 10^{-2}$	$2.1 \times 10^{-2}$
	low alt. monsoon	272.2	$3.5 \times 10^{-2}$	$3.2 \times 10^{-2}$	$2.6 \times 10^{-2}$	$2.4 \times 10^{-2}$	$4.8 \times 10^{-2}$	$4.4 \times 10^{-2}$	$3.6 \times 10^{-2}$	$3.3 \times 10^{-2}$
	high alt. non-monsoon	61.1	$1.4 \times 10^{-2}$	$1.3 \times 10^{-2}$	$1.1 \times 10^{-2}$	$1.0 \times 10^{-2}$	$1.8 \times 10^{-2}$	$1.7 \times 10^{-2}$	$1.4 \times 10^{-2}$	$1.3 \times 10^{-2}$
	low alt. non-monsoon	64.7	$1.4 \times 10^{-2}$	$1.3 \times 10^{-2}$	$1.1 \times 10^{-2}$	$1.0 \times 10^{-2}$	$1.8 \times 10^{-2}$	$1.7 \times 10^{-2}$	$1.4 \times 10^{-2}$	$1.3 \times 10^{-2}$
NETP	high alt. monsoon	87.4	$1.6 \times 10^{-2}$	$1.5 \times 10^{-2}$	$1.2 \times 10^{-2}$	$1.1 \times 10^{-2}$	$2.2 \times 10^{-2}$	$2.0 \times 10^{-2}$	$1.6 \times 10^{-2}$	$1.5 \times 10^{-2}$
	low alt. monsoon	191.4	$2.8 \times 10^{-2}$	$2.6 \times 10^{-2}$	$2.1 \times 10^{-2}$	$2.0 \times 10^{-2}$	$3.8 \times 10^{-2}$	$3.5 \times 10^{-2}$	$2.9 \times 10^{-2}$	$2.6 \times 10^{-2}$
	high alt. non-monsoon	190.9	$2.3 \times 10^{-2}$	$2.1 \times 10^{-2}$	$1.7 \times 10^{-2}$	$1.6 \times 10^{-2}$	$3.1 \times 10^{-2}$	$2.9 \times 10^{-2}$	$2.4 \times 10^{-2}$	$2.2 \times 10^{-2}$
	low alt. non-monsoon	4323.2	$15.1 \times 10^{-2}$	$14.0 \times 10^{-2}$	$11.8 \times 10^{-2}$	$11.0 \times 10^{-2}$	$22.3 \times 10^{-2}$	$20.8 \times 10^{-2}$	$17.8 \times 10^{-2}$	$16.5 \times 10^{-2}$
SETP	high alt. monsoon	823.0	$6.6 \times 10^{-2}$	$6.1 \times 10^{-2}$	$5.1 \times 10^{-2}$	$4.7 \times 10^{-2}$	$9.5 \times 10^{-2}$	$8.7 \times 10^{-2}$	$7.2 \times 10^{-2}$	$6.7 \times 10^{-2}$
	low alt. monsoon	5.2	$0.3 \times 10^{-2}$	$0.2 \times 10^{-2}$	$0.2 \times 10^{-2}$	$0.2 \times 10^{-2}$	$0.4 \times 10^{-2}$	$0.3 \times 10^{-2}$	$0.3 \times 10^{-2}$	$0.3 \times 10^{-2}$
	high alt. non-monsoon	263.6	$3.2 \times 10^{-2}$	$2.9 \times 10^{-2}$	$2.4 \times 10^{-2}$	$2.2 \times 10^{-2}$	$4.3 \times 10^{-2}$	$4.0 \times 10^{-2}$	$3.3 \times 10^{-2}$	$3.0 \times 10^{-2}$
	low alt. non-monsoon	13.7	$0.5 \times 10^{-2}$	$0.5 \times 10^{-2}$	$0.4 \times 10^{-2}$	$0.4 \times 10^{-2}$	$0.7 \times 10^{-2}$	$0.6 \times 10^{-2}$	$0.5 \times 10^{-2}$	$0.5 \times 10^{-2}$
NOTP	high alt. monsoon	1110.9	$6.7 \times 10^{-2}$	$6.2 \times 10^{-2}$	$5.2 \times 10^{-2}$	$4.8 \times 10^{-2}$	$9.8 \times 10^{-2}$	$9.0 \times 10^{-2}$	$7.7 \times 10^{-2}$	$7.1 \times 10^{-2}$
	low alt. monsoon	9.0	$0.4 \times 10^{-2}$	$0.4 \times 10^{-2}$	$0.3 \times 10^{-2}$	$0.3 \times 10^{-2}$	$0.5 \times 10^{-2}$	$0.5 \times 10^{-2}$	$0.4 \times 10^{-2}$	$0.4 \times 10^{-2}$
	high alt. non-monsoon	249.4	$3.1 \times 10^{-2}$	$2.8 \times 10^{-2}$	$2.3 \times 10^{-2}$	$2.1 \times 10^{-2}$	$4.2 \times 10^{-2}$	$3.9 \times 10^{-2}$	$3.2 \times 10^{-2}$	$2.9 \times 10^{-2}$
	low alt. non-monsoon	368.6	$4.0 \times 10^{-2}$	$3.6 \times 10^{-2}$	$3.0 \times 10^{-2}$	$2.8 \times 10^{-2}$	$5.5 \times 10^{-2}$	$5.0 \times 10^{-2}$	$4.2 \times 10^{-2}$	$3.8 \times 10^{-2}$
NOTP	high alt. non-monsoon	89.1	$1.8 \times 10^{-2}$	$1.6 \times 10^{-2}$	$1.3 \times 10^{-2}$	$1.2 \times 10^{-2}$	$2.3 \times 10^{-2}$	$2.1 \times 10^{-2}$	$1.7 \times 10^{-2}$	$1.6 \times 10^{-2}$
	low alt. non-monsoon	138.3	$2.4 \times 10^{-2}$	$2.2 \times 10^{-2}$	$1.8 \times 10^{-2}$	$1.6 \times 10^{-2}$	$3.1 \times 10^{-2}$	$2.8 \times 10^{-2}$	$2.4 \times 10^{-2}$	$2.2 \times 10^{-2}$

973 <sup>1</sup>Six sub-regions: Himalayas (HIMA), central Tibetan Plateau (CTP), northwestern Tibetan Plateau (NWTP),  
 974 northeastern Tibetan Plateau (NETP), southeastern Tibetan Plateau (SETP), and north of Tibetan Plateau (NOTP).  
 975 Each sub-region is further divided into high (>5200 m) and low (<5200 m) altitudes.  
 976  
 977  
 978  
 979  
 980  
 981  
 982  
 983

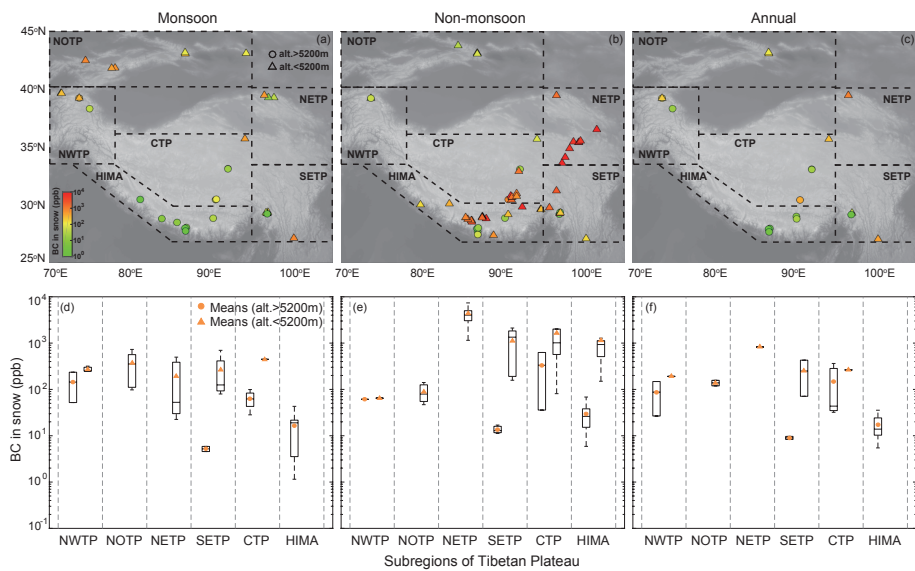
Deleted: ¶

985 **Table 3.** Regional and seasonal mean BC-induced all-sky surface radiative effects ( $W m^{-2}$ ) for  
 986 fresh snow over the Tibetan Plateau during 2000–2015. See Table S4 for results of aged snow.

Region <sup>1</sup>		Season	Fresh snow ( $R_e = 100 \mu m$ )							
			External mixing				Internal mixing			
			Sphere	Spheroid	Hexagonal plate	Koch snowflake	Sphere	Spheroid	Hexagonal plate	Koch snowflake
HIMA	high alt.	monsoon	1.4	1.3	1.1	1.0	2.0	1.8	1.5	1.4
	low alt.		2.0	1.8	1.5	1.4	2.6	2.4	2.0	1.8
	high alt.	non-monsoon	16.2	15.0	12.8	11.9	23.9	22.2	19.0	17.6
	low alt.		1.5	1.4	1.2	1.1	2.0	1.8	1.5	1.4
CTP	high alt.	monsoon	4.2	3.9	3.2	3.0	5.6	5.1	4.2	3.9
	low alt.		14.7	13.5	11.2	10.3	20.5	18.7	15.6	14.3
	high alt.	non-monsoon	7.7	7.0	5.8	5.3	10.6	9.7	8.1	7.4
	low alt.		17.3	16.2	13.8	12.8	25.8	24.1	20.6	19.1
NWTP	high alt.	monsoon	7.2	6.6	5.5	5.0	9.7	8.8	7.3	6.7
	low alt.		11.3	10.3	8.5	7.8	15.3	14.0	11.6	10.7
	high alt.	non-monsoon	2.7	2.5	2.1	1.9	3.6	3.2	2.7	2.4
	low alt.		2.7	2.5	2.1	1.9	3.6	3.3	2.7	2.5
NETP	high alt.	monsoon	3.9	3.5	2.9	2.7	5.1	4.7	3.9	3.5
	low alt.		6.6	6.1	5.0	4.6	9.0	8.2	6.8	6.2
	high alt.	non-monsoon	6.5	6.0	5.0	4.6	8.9	8.2	6.8	6.3
	low alt.		30.7	28.4	24.1	22.3	45.4	42.3	36.2	33.6
SETP	high alt.	monsoon	15.3	14.0	11.7	10.7	21.8	20.0	16.7	15.4
	low alt.		0.7	0.6	0.5	0.5	1.0	0.9	0.8	0.7
	high alt.	non-monsoon	8.5	7.7	6.4	5.9	11.5	10.6	8.8	8.0
	low alt.		1.2	1.1	0.9	0.8	1.5	1.4	1.1	1.0
NOTP	high alt.	monsoon	14.5	13.4	11.4	10.5	21.3	19.7	16.6	15.4
	low alt.		0.9	0.8	0.7	0.6	1.3	1.2	1.0	0.9
	high alt.	non-monsoon	7.3	6.6	5.5	5.0	9.9	9.0	7.5	6.9
	low alt.		11.2	10.2	8.4	7.7	15.4	14.1	11.7	10.7
NOTP	high alt.	monsoon	2.9	2.7	2.2	2.0	3.8	3.5	2.9	2.6
	low alt.		4.8	4.4	3.6	3.3	6.4	5.8	4.8	4.4
	high alt.	non-monsoon	2.9	2.7	2.2	2.0	3.8	3.5	2.9	2.6
	low alt.		4.8	4.4	3.6	3.3	6.4	5.8	4.8	4.4

987 <sup>1</sup>Six sub-regions: Himalayas (HIMA), central Tibetan Plateau (CTP), northwestern Tibetan Plateau (NWTP),  
 988 northeastern Tibetan Plateau (NETP), southeastern Tibetan Plateau (SETP), and north of Tibetan Plateau (NOTP).  
 989 Each sub-region is further divided into high (>5200 m) and low (<5200 m) altitudes.

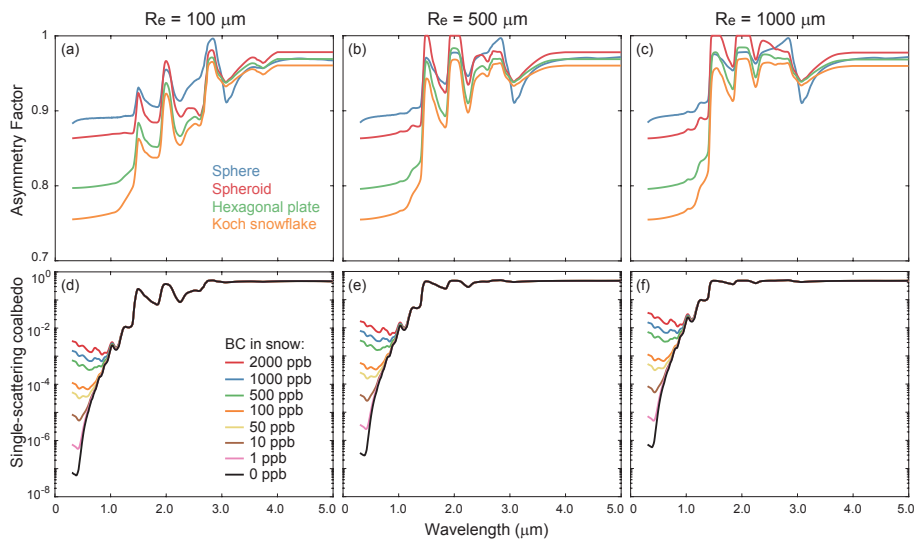
990  
 991  
 992  
 993  
 994  
 995  
 996  
 997



998  
999

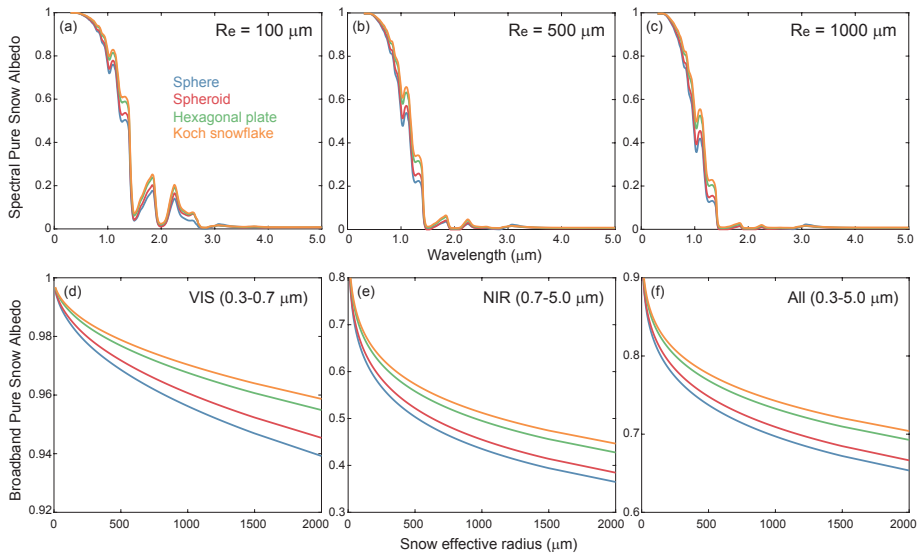
1000 **Figure 1.** Observed BC concentrations in snow over the Tibetan Plateau (TP) during (a, d)  
1001 monsoon, (b, e) non-monsoon, and (c, f) annual periods in 2000–2015 (see Table S1 for details).  
1002 (a–c) Spatial distributions of seasonal mean BC concentrations at altitudes >5200 m (circles) and  
1003 <5200 m (triangles) in six sub-regions, including northwestern TP (NWTP), north of TP (NOTP),  
1004 northeastern TP (NETP), southeastern TP (SETP), central TP (CTP), and Himalayas (HIMA). (d–  
1005 f) Boxplots of observed BC concentrations in snow (shown in a–c) within each sub-region, with  
1006 medians (middle bars), interquartile ranges (between 25<sup>th</sup> and 75<sup>th</sup> percentiles; boxes), and  
1007 maxima/minima (whiskers) within  $\pm 1.5 \times$  interquartile ranges. Some boxplots are shrunk due to  
1008 limited samples. Results for altitudes >5200 m and <5200 m are shown as left and right boxplots  
1009 within each sub-region, respectively, with circles and triangles indicating mean values. Note that  
1010 some sub-regions only have observations at altitudes >5200 m or <5200 m.

1011  
1012  
1013  
1014  
1015  
1016  
1017  
1018  
1019  
1020  
1021  
1022  
1023



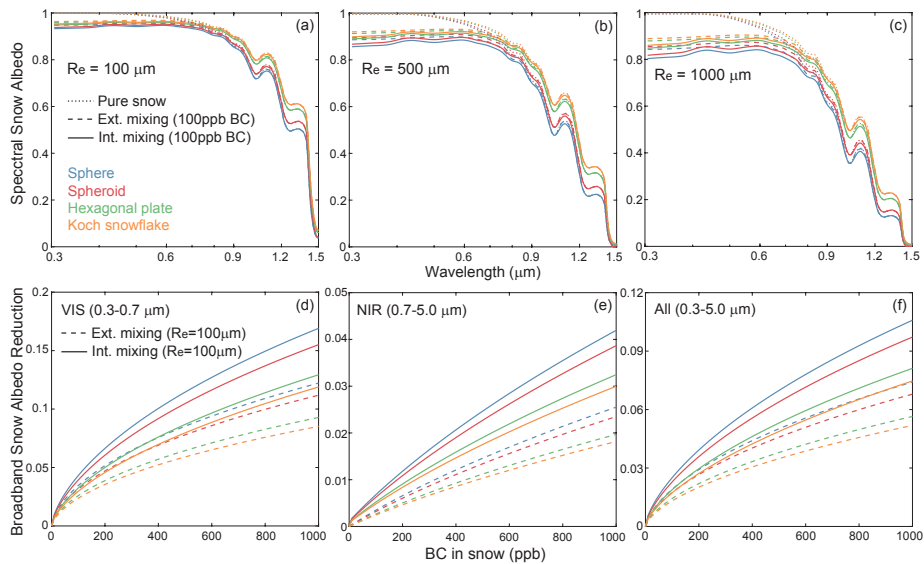
1024  
 1025  
 1026  
 1027  
 1028  
 1029  
 1030  
 1031  
 1032  
 1033  
 1034  
 1035  
 1036  
 1037  
 1038  
 1039  
 1040  
 1041  
 1042  
 1043  
 1044  
 1045  
 1046  
 1047  
 1048  
 1049  
 1050

**Figure 2.** (a–c) Spectral (0.3–5 μm) asymmetry factors of pure snow with effective radii ( $R_e$ ) of (a) 100, (b) 500, and (c) 1000 μm for sphere (blue), spheroid (red), hexagonal plate (green), and Koch snowflake (orange) derived from the updated SNICAR model. (d–f) Spectral single-scattering coalbedo of snow grains internally mixed with different BC concentrations (indicated by different colors) for snow effective radii ( $R_e$ ) of (d) 100, (e) 500, and (f) 1000 μm derived from the updated SNICAR model. Note that the y-axes in (d–f) are in logarithmic scales.



1051  
 1052  
 1053  
 1054  
 1055  
 1056  
 1057  
 1058  
 1059  
 1060  
 1061  
 1062  
 1063  
 1064  
 1065  
 1066  
 1067  
 1068  
 1069  
 1070  
 1071  
 1072  
 1073  
 1074  
 1075  
 1076  
 1077

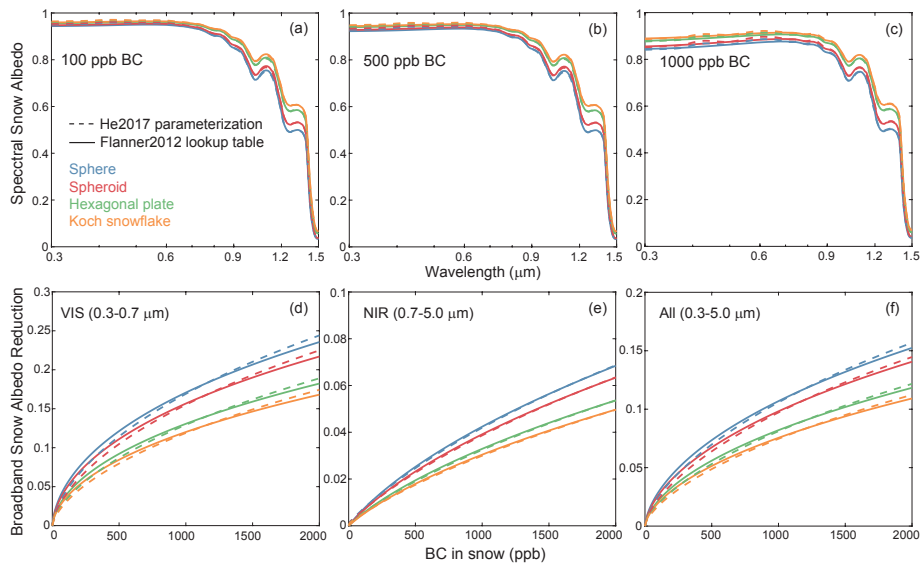
**Figure 3.** (a–c) Spectral (0.3–5 μm) direct-beam albedo of pure semi-infinite snow layers with effective radii ( $R_e$ ) of (a) 100, (b) 500, and (c) 1000 μm for sphere (blue), spheroid (red), hexagonal plate (green), and Koch snowflake (orange) based on the updated SNICAR model. (d–f) Same as (a–c), but for broadband albedo as a function of snow effective radius ( $R_e$ ) at (d) visible (VIS, 0.3–0.7 μm), (e) near-infrared (NIR, 0.7–5 μm), and (f) all (0.3–5 μm) wavelengths. The results for diffuse snow albedo are shown in Fig. S1.



1078  
1079

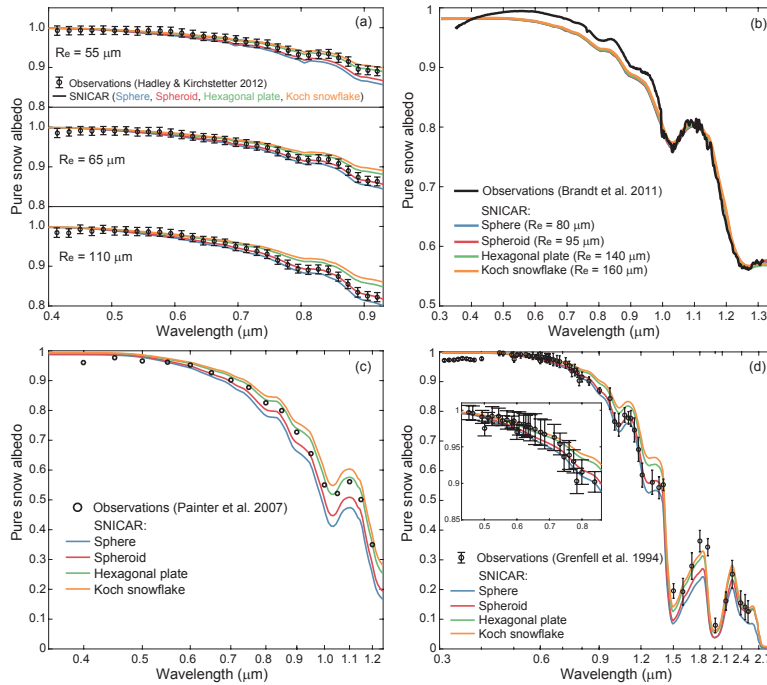
1080 **Figure 4.** (a–c) Spectral (0.3–1.5 μm) direct-beam albedo of semi-infinite snow layers with  
 1081 effective radii ( $R_e$ ) of (a) 100, (b) 500, and (c) 1000 μm for pure snow (dotted lines), snow  
 1082 externally mixed with 100 ppb BC (dashed lines), and snow internally mixed with 100 ppb BC  
 1083 (solid lines) with shapes of sphere (blue), spheroid (red), hexagonal plate (green), and Koch  
 1084 snowflake (orange) based on the updated SNICAR model. The results for 1000 ppb BC and diffuse  
 1085 snow albedo are shown in Fig. S2. (d–f) Same as (a–c), but for broadband albedo reduction as a  
 1086 function of BC concentration in snow with  $R_e$  of 100 μm at (d) visible (VIS, 0.3–0.7 μm), (e)  
 1087 near-infrared (NIR, 0.7–5 μm), and (f) all (0.3–5.0 μm) wavelengths. The results for snow with  $R_e$  of 500  
 1088 and 1000 μm and diffuse albedo reductions are shown in Figs. S3 and S4, respectively.

1089  
1090  
1091  
1092  
1093  
1094  
1095  
1096  
1097  
1098  
1099  
1100  
1101  
1102  
1103



1104  
 1105  
 1106  
 1107  
 1108  
 1109  
 1110  
 1111  
 1112  
 1113  
 1114  
 1115  
 1116  
 1117  
 1118  
 1119  
 1120  
 1121  
 1122  
 1123  
 1124  
 1125  
 1126  
 1127  
 1128  
 1129

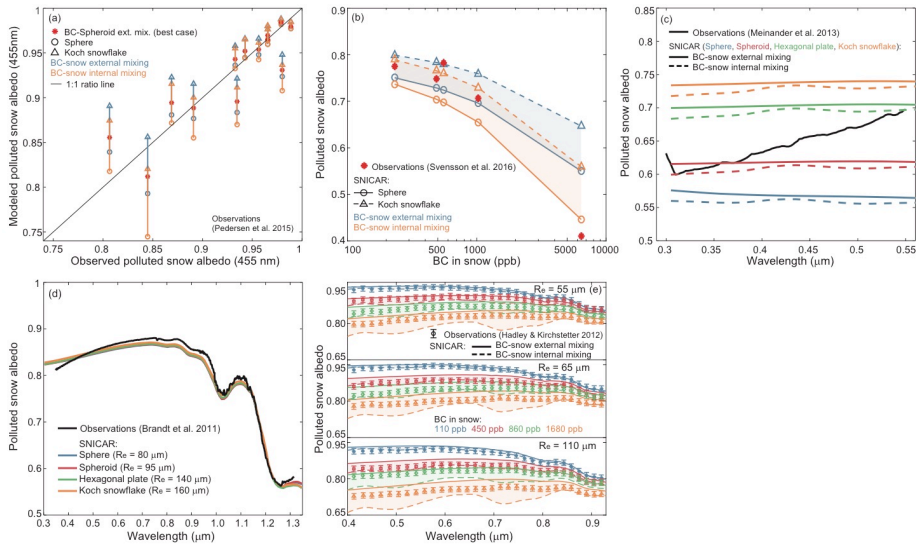
**Figure 5.** Comparisons of SNICAR simulated direct-beam albedo of semi-infinite snow layers between using the Flanner et al. (2012) lookup table (solid lines) and the He et al. (2017b) parameterization (dashed lines) for BC internally mixed with snow grains with an effective radius of 100  $\mu\text{m}$  for sphere (blue), spheroid (red), hexagonal plate (green), and Koch snowflake (orange). (a–c) Spectral (0.3–1.5  $\mu\text{m}$ ) snow albedo for BC concentrations of (a) 100, (b) 500, and (c) 1000 ppb. (d–f) Broadband snow albedo reduction as a function of BC concentration in snow at (d) visible (VIS, 0.3–0.7  $\mu\text{m}$ ), (e) near-infrared (NIR, 0.7–5  $\mu\text{m}$ ), and (f) all (0.3–5  $\mu\text{m}$ ) wavelengths. The results for snow effective radii of 500 and 1000  $\mu\text{m}$  are shown in Figs. S5 and S6, respectively.



1130  
 1131  
 1132  
 1133  
 1134  
 1135  
 1136  
 1137  
 1138  
 1139  
 1140  
 1141  
 1142  
 1143  
 1144  
 1145  
 1146  
 1147  
 1148  
 1149  
 1150  
 1151

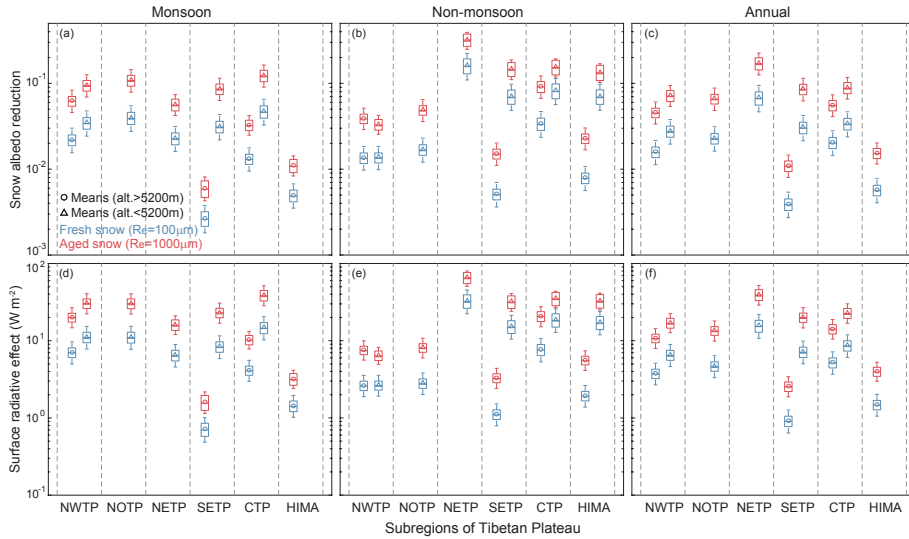
**Figure 6.** Comparisons of spectral pure snow albedo from observations (black) and SNICAR simulations using observed snowpack properties (see Table 1 and text for details) and assuming sphere (blue), spheroid (red), hexagonal plate (green), and Koch snowflake (orange). (a) Observations are obtained from laboratory measurements (Hadley and Kirchstetter, 2012). (b) Observations are obtained from open-field experiments in New York (Brandt et al., 2011). The effective radii ( $R_e$ ) for each snow shape are obtained to best match observations at wavelengths of 1–1.3  $\mu\text{m}$ . (c) Observations are obtained from field measurements over Rocky Mountains (Painter et al., 2007). (d) Observations are obtained from field measurements at the South Pole (Grenfell et al., 1994).

Deleted: ¶



1153  
 1154  
 1155  
 1156  
 1157  
 1158  
 1159  
 1160  
 1161  
 1162  
 1163  
 1164  
 1165  
 1166  
 1167  
 1168  
 1169  
 1170  
 1171  
 1172  
 1173  
 1174  
 1175  
 1176  
 1177  
 1178  
 1179

**Figure 7.** Comparisons of BC-polluted snow albedo from observations and SNICAR simulations using observed snowpack properties (see Table 1 and text for details). (a) Observations (x-axis) are obtained from field measurements in the Arctic (Pedersen et al., 2015). Model results (y-axis) for spheres (circles) and Koch snowflake (triangles) are shown as lower and upper limits for shape effects, along with BC-snow external (blue) and internal (orange) mixing. Also shown is the best case (red asterisks; BC-spheroid external mixing) that matches observations. (b) Observations (red asterisks; broadband albedo for 0.285–2.8 μm) are obtained from open-field experiments in Finland (Svensson et al., 2016). Model results for spheres (circles) and Koch snowflake (triangles) are shown as lower and upper limits for shape effects, along with BC-snow external (blue) and internal (orange) mixing. (c) Observations (black lines) are obtained from field measurements in the European Arctic (Meinander et al., 2013). Model results assuming sphere (blue), spheroid (red), hexagonal plate (green), and Koch snowflake (orange) along with BC-snow external (dashed lines) and internal (solid lines) are shown. (d) Observations (black) are obtained from open-field experiments in New York (Brandt et al., 2011). BC is assumed to be externally mixed with snow spheres (blue), spheroids (red), hexagonal plates (green), and Koch snowflakes (orange). The effective radii ( $R_e$ ) for each snow shape are obtained to best match observations at wavelengths of 1–1.3 μm. (e) Observations (circles) are obtained from laboratory measurements (Hadley and Kirchstetter, 2012). BC is assumed to be externally (solid lines) and internally (dashed lines) mixed with snow spheres.



1180  
 1181  
 1182  
 1183  
 1184  
 1185  
 1186  
 1187  
 1188  
 1189  
 1190  
 1191  
 1192  
 1193  
 1194  
 1195  
 1196  
 1197  
 1198  
 1199

**Figure 8.** Regional and seasonal mean BC-induced all-sky snow albedo reductions and surface radiative effects during (a, d) monsoon, (b, e) non-monsoon, and (c, f) annual periods in 2000–2015 over six Tibetan Plateau (TP) sub-regions (see Fig. 1), including northwestern TP (NWTP), north of TP (NOTP), northeastern TP (NETP), southeastern TP (SETP), central TP (CTP), and Himalayas (HIMA). (a–c) Boxplots of mean snow albedo reductions within each sub-region based on SNICAR simulations using the observed BC concentrations in snow (Fig. 1), snow thicknesses, and snow densities (see text for details). Results for altitudes >5200 m and <5200 m are shown as left and right boxplots within each sub-region, respectively, with circles and triangles indicating mean values. Model results assume BC externally and internally mixed with spheres, spheroids, hexagonal plates, and Koch snowflakes for fresh (blue,  $R_e = 100 \mu\text{m}$ ) and aged (red,  $R_e = 1000 \mu\text{m}$ ) snow. Each data point used for the boxplot is the sub-regional average assuming a type of snow shape and BC-snow mixing, and hence the boxplot indicates the variation caused by effects of snow shape and BC-snow mixing state. Note that some sub-regions only have BC observations at altitudes >5200 m or <5200 m (see Fig. 1). (d–f) Same as (a–c), but for BC-induced all-sky surface radiative effects caused by the snow albedo reductions shown in (a–c). Calculations use the surface downward solar radiation and cloud cover fraction from the MERRA-2 reanalysis fields (see text and Table S2 for details).